RESEARCH ARTICLE

JCN RESEARCH IN SYSTEMS NEUROSCIENCE
THE JOURNAL OF COMPARATIVE NEUROLOGY WILEY

Distinct burst properties contribute to the functional diversity of thalamic nuclei

Nidhi Vasant Desai | Carmen Varela [ORCID]

Psychology Department, Jupiter Life Sciences Initiative, Florida Atlantic University, Boca Raton, Florida, USA

Correspondence
Carmen Varela, Florida Atlantic University, Boca Raton, FL 33431.
Email: carmenv.work@gmail.com

Abstract

Thalamic neurons fire spikes in two modes, burst and tonic. The function of burst firing is unclear, but the evidence suggests that bursts are more effective at activating cortical cells, and that postinhibition rebound bursting contributes to thalamocortical oscillations during sleep. Bursts are considered stereotyped signals; however, there is limited evidence regarding how burst properties compare across thalamic nuclei of different functional or anatomical organization. Here, we used whole-cell patch clamp recordings and compartmental modeling to investigate the properties of bursts in six sensory thalamic nuclei, to study the mechanisms that can lead to different burst properties, and to assess the implications of different burst properties for thalamocortical transmission and oscillatory functions. We found that bursts in higher-order cells on average had higher number of spikes and longer latency to the first spike. Additionally, burst features in first-order neurons were determined by sensory modality. Shifting the voltage-dependence and density of the T-channel conductance in a compartmental model replicates the burst properties from the intracellular recordings, pointing to molecular mechanisms that can generate burst diversity. Furthermore, the model predicts that bursts with higher number of spikes will drastically reduce the effectiveness of thalamocortical transmission. In addition, the latency to burst limited the rebound oscillatory frequency in modeled cells. These results demonstrate that burst properties vary according to the thalamocortical hierarchy and with sensory modality. The findings imply that, while in burst mode, thalamocortical transmission and firing frequency will be determined by the number of spikes and latency to burst.

KEYWORDS
burst, first order, higher order, oscillation, sensory, thalamocortical, thalamus

1 | INTRODUCTION

Neurons within the nuclei of the thalamus present regional specializations overlaid onto a functional architecture of shared connectivity and cellular intrinsic properties (Bickford, 2015; Guillery & Sherman, 2002; Halassa & Acsády, 2016; Halassa & Sherman, 2019; Jones, 1998; Phillips et al., 2019). One of the shared properties of thalamic neurons is that they fire in two fundamentally different modes, *tonic* mode when they are depolarized, and *burst* mode, when hyperpolarized (Gutierrez et al., 2001; Huguenard, 1996; Jahnsen &

Llinás, 1984a, 1984b; Perez-Reyes, 2003). Bursts across the thalamus are considered fairly stereotyped signals that provide enhanced detectability of sensory stimuli during wakefulness and contribute to the generation of rhythms during sleep (Crunelli et al., 2018; Guido et al., 1992; Guido & Weyand, 1995; Llinás & Steriade, 2006; Nicolelis, 2005; Reinagel et al., 1999; X. Wang et al., 2007; Whitmire et al., 2016). However, it is unclear whether burst properties vary in different thalamic regions according to their connectivity with cortex, to the sensory modality they process or to both.

Burst firing requires a relatively prolonged hyperpolarization of the cell to deinactivate low-threshold, T-type, calcium channels, which can then be activated through depolarization to produce a rapid succession of sodium-potassium action potentials (Jahnsen & Llinás, 1984a, 1984b; Suzuki & Rogawski, 1989). The same time course that deinactivates the T-channels helps replenish neurotransmitter in the presynaptic terminals of thalamocortical driver synapses, which contributes to increase the effectiveness of burst spikes, compared to tonic firing, at activating postsynaptic cortical cells (Gil et al., 1997; Hu & Agmon, 2016; Krahe & Gabbiani, 2004; S. M. Sherman, 2001; Swadlow & Gusev, 2001; Viaene et al., 2011a, 2011b, 2011c). The number of spikes in the burst also determines thalamocortical transmission; thalamic bursts with more than one spike were more effective at activating pyramidal cells and somatostatin interneurons in the somatosensory cortex (Hu & Agmon, 2016). Therefore, if cells in different parts of the thalamus produce bursts with different delays after removal from hyperpolarization, or with different numbers of spikes, it will have implications for the effective transmission of information to cortex.

In addition, thalamic cells burst at higher rates during sleep (Fourment et al., 1984; Llinás & Steriade, 2006; Varela & Wilson, 2020; Weyand et al., 2001), when they contribute to the generation of sleep spindles, hallmark oscillations of non-rapid eye movement (NREM) sleep that provide temporal windows for coordination of thalamocortical and hippocampal networks (Astori et al., 2011; Bal et al., 1995; Sirota et al., 2003; Staresina et al., 2015; Steriade et al., 1985, 1987; Varela & Wilson, 2020). Bursts with different properties (latency to burst, number of spikes/burst, and intraburst spike frequency) could thus influence thalamic function across behavioral states, the detection of sensory stimuli during wakefulness and the oscillatory coupling of thalamocortical networks during sleep.

There are reports of a larger T-current in cells of the lateral posterior (LP) nucleus compared to cells in the lateral geniculate (Li et al., 2003; Wei et al., 2011) and of bursts with more spikes in cells of the ventral posterior (VP) compared to the posterior medial nucleus (Landisman & Connors, 2007; Slézia et al., 2011). Cells in higher order were more likely to fire spikes in bursts compared to cells in first-order (FO) nuclei (Ramcharan et al., 2005), and the propensity to burst was also higher in thalamic reticular nucleus (TRN) cells connected to sensory nuclei compared to TRN cells connected to higher-order (HO) dorsal thalamus (Clemente-Perez et al., 2017; Fernandez et al., 2018; Li et al., 2020; Martinez-Garcia et al., 2020). These results suggest that burst properties vary according to the functional organization of the thalamus. One hypothesis is that burst properties will be

congruent with the hierarchical level of the network in which a thalamic nucleus is embedded (FO or HO, core or matrix; Guillery & Sherman, 2002; Jones, 1998). It is also possible that the type of information processed by a given nucleus determines the firing properties of its thalamocortical cells, in which case burst properties may be different in nuclei processing different sensory input. To shed light on these hypotheses, we studied the properties of bursts recorded intracellularly (whole-cell patch clamp; rat brain slices) in six thalamic nuclei, one FO and one HO nucleus in each of three sensory systems (somatosensory, visual, and auditory). We then used compartmental models to gain insight on the underlying molecular mechanisms and functional implications of the burst diversity we observed in the in vitro data.

2 | MATERIALS AND METHODS

2.1 | Animal subjects

We used P11 to 18 days old Sprague–Dawley rats of both sexes (Harlan Sprague–Dawley, Indianapolis, IN). The animals were euthanized via decapitation as part of the procedure of slice preparation. All the experimental procedures were approved according to the animal care guidelines of The University of Chicago.

2.2 | In vitro data collection

Intracellular whole-cell patch clamp recordings were performed in current clamp configuration in six thalamic nuclei (Varela & Sherman, 2009, 2007): three FO nuclei (lateral geniculate nucleus, ventral posterior nucleus [VP], and ventral medial geniculate body [vMGB]) and three HO nuclei (lateral posterior nucleus [LP], posterior medial nucleus [POm], and dorsal medial geniculate body [dMGB]). Briefly, 400 μm coronal slices, which are unlikely to preserve connections with the TRN, were prepared from the brains of P11-18 rats and were maintained in a beaker with artificial cerebrospinal fluid (ACSF composed of, in mM: 125 NaCl, 25 NaHCO$_3$, 3 KCl, 1.25 NaH$_2$PO$_4$, 1 MgCl$_2$, 2 CaCl$_2$, and 25 glucose) supplemented with 95% O2–5% CO$_2$. We prepared coronal slices at anteroposterior coordinates that contained the nuclei of interest; the slices were maintained at 30°C for ~30 min after sectioning, then kept at room temperature for the duration of the experiment. Recordings were performed in a standard patch clamp rig under microscope observation and cells were selected with the aid of the microscope. The inflow rate of ACSF (warmed to 30 ± 2°C before entering the chamber holding the slice) was kept at ~2 ml/min. The micropipette solution contained (in mM): 117 KGluconate, 13 KCl, 10 (4-(2-hydroxyethyl)-1-piperazineethanesulfonic acid) (HEPES), 2 Na$_2$ATP, 0.4 Na$_3$GTP, 1 MgCl$_2$, 0.07 CaCl$_2$, and 0.1 ethylene glycol tetra-acetic acid (EGTA). Signals were amplified and filtered (30 kHz) with an Axoclamp 2A amplifier, digitized with the Digidata 1200B converter and sampled at 10 kHz (Axon Instruments, Union City, CA). Cells with input resistance

below 100 MOhms or access resistance above 30 MOhms were discarded. Square current pulses (median number of pulses per cell = 7, inter-quartile-range [IQR] = 5–8 pulses) of decreasing negative current (average starting pulse −0.41 ± 0.13 nA, subsequent pulses increased by −0.05 ± 0.01 nA) and ≥ 400 ms duration were used to hyperpolarize each cell through a range of physiological voltages from −62.44 to −128 mV from an initial resting potential of −61.41 ± 4.98 mV to induce rebound bursts upon release from hyperpolarization. The burst data resulting from the current injection protocol were collected before the cells were tested as part of the experiments by Varela and Sherman (2007, 2009), and so no modulators or drugs were applied to the cell before or during the current injection protocols used for burst induction used for this manuscript. Only one cell was recorded in each brain slice.

2.3 | In vitro burst analysis

For every current injection applied to a cell, the recorded voltage trace was analyzed to quantify the features discussed in Section 3. Resting potential was calculated as the average membrane potential in the first 200 ms of the voltage trace, before the negative current pulse started. We estimated the hyperpolarization level preceding burst induction for each current injection pulse as the average membrane potential in the 100 ms immediately before the end of the negative current injection pulse. A burst was identified as a rebound low-threshold spike (LTS) with at least one Na^+-K^+ spike. For each burst produced after current injection, we quantified several features: number of spikes in the burst, interspike interval (ISI), latency to the first spike, and decay time constant. The spikes were detected in the voltage traces using the *findpeaks* function in Matlab, followed by visual inspection. We defined a pulse as producing no burst when no Na^+-K^+ spikes were observed after the hyperpolarization; in most cases, pulses that did not induce a burst were ohmic responses and had no LTS associated with them. Only seven pulses of current injection, one in each of seven different cells evoked an LTS with no Na^+-K^+ spikes). We never observed tonic firing when cells were released from hyperpolarization. We used the ISIs to estimate the first ISI frequency in spikes/s. Bursts with only one spike were excluded from within-burst spike frequency calculations. Spike frequency adaptation within the burst was calculated as the percent change from first to last ISI frequency for cells with at least four spikes. The latency was calculated as the time from the end of the negative current pulse to the peak of the first spike in the burst. We estimated the decay time constant by fitting the sum of two exponential curves to the voltage trace after the last spike in the burst (Equation (1)). There were two components to the decay, the slower decay time constant was too long (average = 34,662 ms) to explain the drop in voltage following the transient T current. Therefore, we considered the faster component as the estimate for the decay time constant for the T-current dynamics.

$$V = a * \exp(-\tau_{fast} * t) + b * \exp(-\tau_{slow} * t) \tag{1}$$

where V is the membrane potential and t is the time.

2.4 | Compartmental models

We used the DynaSim toolbox in Matlab (Sherfey et al., 2018) to implement a single compartment model (Equations (2) and (3)) that includes the most relevant voltage-dependent currents of thalamic cells and reproduces the essential features of burst and tonic firing of thalamocortical cells. The membrane potential in the compartment was described by:

$$C_m \frac{dV}{dt} = I_{app} - I_K - I_{Na} - I_{Leak} - I_{KLeak} - I_T - I_H \tag{2}$$

where V is the membrane potential, C_m is the membrane capacitance (1 μF/cm^2), I_{Na} and I_K are the sodium and potassium currents responsible for the action potential, I_T is the low-threshold calcium current responsible for burst firing. I_{app} (in μA/cm^2) was used to simulate current injection into the cell. In this model, the voltage-dependent currents are variants of the same generic Hodgkin–Huxley (HH) equation (Hodgkin & Huxley, 1952):

$$I_j = \bar{g}_j \, m^M \, h^N \, (V - E_j) \tag{3}$$

which expresses each current, I_j, as the product of the maximum conductance, g_j, activation, m, and inactivation, h, variables, and the difference between the membrane and reversal potentials ($V – E_j$). We chose parameters as in the study by Benita et al. (2012), Destexhe et al. (1996), and Soplata et al. (2017), with modifications to I_{Leak} and I_{KLeak}. Here, we opted for a more depolarized model, which may be more similar to wakefulness conditions. We used g_{KLeak} = 0.014 mS/cm^2, E_{KLeak} = E_{Leak} = −60 mV. g_T was varied between 0.15 and 1 mS/cm^2 in simulations where we shifted the activation and inactivation curves. For simulations for burst oscillatory frequency (Section 3.8), g_T was kept at 1 mS/cm^2.

In one of our models, we also implement a neurotransmitter release probability variable (Benita et al., 2012). This variable remains at a steady-state probability of release, until a presynaptic spike reduces the release probability by a fraction of 0.1 and then it recovers with a time constant of 400 ms. To test the implications of different synaptic release probabilities for thalamocortical transmission, we connected the single compartment model of the thalamic cell with a compartmental model of either one pyramidal cell or an interneuron, with the same currents and parameters used in the network model of Benita et al. (2012), except we lowered the equilibrium potential for the leak current in the Pyramidal cell to −70 mV (Benita et al., 2012 used −60.95 mV) to increase the dynamic range of excitatory postsynaptic potential (EPSP) amplitudes evoked by the thalamic cell. The pyramidal cell model was a two-compartment model with soma (including leak, A-type, and slow potassium currents, as well as sodium and potassium action potential generating currents) and one dendrite (including inwardly rectifying potassium current, persistent sodium current, slow calcium-dependent potassium current, and high-threshold calcium current). The interneuron had a single compartment with potassium leak current and the sodium and

potassium action potential generating currents; the thalamic cell model was connected either to the pyramidal cell dendrite or to the interneuron through an α-amino-3-hydroxy-5-methyl-4-isoxazole propionic acid (AMPA) current. The scripts for the models used in this article are available at https://github.com/nidhi-desai/thalamic-distinct-burst. The code implementing the individual currents and model specifications is available at https://github.com/asoplata/dynasim-extended-benita-model.

2.5 | Statistical analyses

For population results, we report the mean and *SD* in the text and display the population distribution of the calculated metrics in figures in box and whisker plots. Because the distributions of the metrics we calculated were non-Gaussian and the samples sizes small, we opted for nonparametric statistical tests. We used the Kruskal–Wallis test for group comparisons. We used Kruskal–Wallis test with post hoc analysis using Tukey–Kramer correction for multiple comparison tests to test for differences in burst properties across cells. Also, we used the Wilcoxon signed-rank test to compare paired data under difference conditions.

To estimate the change in spikes per burst and within-burst spike frequency (spikes/s) as a function of hyperpolarization, we used a generalized linear model (GLM; Equations (4) and (5); Kramer & Eden, 2016; https://github.com/Mark-Kramer/Case-Studies-Kramer-Eden) to estimate the spikes/burst or their frequency (μ) as a linear function of the hyperpolarization level (X) induced by the negative current pulses, assuming a Poisson distribution of errors (Equation (4)). The model included two parameters, β_0, representing the expected value of the dependent variable at baseline membrane potential, and β_1, representing the expected change in the dependent variable for each unit of change in the covariate. The model was fit using a maximum likelihood approach to estimate the values of the parameters that best predict the data. Parameter estimates based on this method are often normally distributed, which allowed us to define 95% confidence intervals at ±2 times the standard error for each parameter (obtained from Matlab's maximum likelihood estimation). From the fitted model, we estimated the change in the response variable (spikes/burst, spike frequency) per mV change in membrane potential from the equivalent equation (5). The Wald test was used to test the significance of the hyperpolarization level parameter (β_1). The Wald test assesses whether a parameter is significantly different from 0, in which case it is considered to have a significant contribution to the model (Kramer & Eden, 2016). We used the GLM to characterize the relation between burst properties and hyperpolarization in each individual cell; because we did not attempt to develop general predictive models, we did not include regularization parameters.

$$\log(\mu) = \beta_0 + \beta_1 X \qquad (4)$$

$$\mu = \exp(\beta_0 + \beta_1 X) \qquad (5)$$

In the analyses in which we systematically shifted the levels of T-channel conductance and its voltage dependence, we used the distributions of burst properties in each nucleus from our in vitro data (Figures 1(d) and 4(b)) to determine whether the burst properties obtained from model simulations more closely resembled bursts from FO or from HO nuclei. First, we calculated the probability density functions for the distribution of spikes per burst and latency for each of the six nuclei; for each of the simulated bursts, we then calculated the probability of seeing a burst with the same number of spikes per burst and latency in each of the six nuclei (by multiplying the probability of observing a burst with the same number of spikes in each nucleus by the probability of observing a burst with the same latency). We used the nucleus with the highest combined probability to determine whether FO or HO nuclei most closely resembled the burst properties produced in the model by a particular combination of T-channel conductance and voltage dependence.

3 | RESULTS

We recorded intracellularly in current clamp mode from 91 cells in six nuclei of the dorsal thalamus (sample size per nucleus in Table 1). All of the nuclei are sensory regions of the thalamus; three of the nuclei (dorsal lateral geniculate nucleus [dLGN], VP, vMGB) are FO in the visual, somatosensory, and auditory systems, whereas the other three (LP, POm, and dMGB) are HO functionally associated with the same sensory systems (Guillery & Sherman, 2002; Prasad et al., 2020). Thus, this sample allowed us to investigate how the properties of bursts resulting from rebound after hyperpolarization relate to thalamocortical connectivity and to sensory modality. We applied steps of negative current to induce a rebound burst at the end of the current step (Figure 1(a)). For each burst, we quantified several features to characterize its dynamics, such as the number of spikes, within-burst frequency of ISIs, latency to the first spike (Figure 1(b)) and the decay time from the last spike in the burst to the baseline membrane potential (see Section 2 for details).

3.1 | Visual and auditory thalamic neurons in FO nuclei produce bursts with less spikes than in HO nuclei

Some cells were more likely to produce a burst when released from hyperpolarization. We found that 26% of the negative current pulses did not induce a rebound burst (defined as a LTS—with at least one Na$^+$-K$^+$ spike), even though the average hyperpolarization level during those pulses was −89.5 ± 15.17 mV. The percentage of pulses that did not induce a burst was different across thalamic nuclei, ranging from 2% in VP to 39% in dLGN (see Table 1 for all nuclei). The "no-burst" percentages include a few current pulses that evoked an LTS but no Na$^+$-K$^+$ action potentials, something that was rare in our sample (seven cells from vMGB, dMGB, dLGN, and VP produced an LTS with no Na$^+$-K$^+$

FIGURE 1 Number of spikes in bursts evoked by hyperpolarization of TC cells in different nuclei. (a) Cells were recorded in current clamp and injected with step pulses to evoke rebound bursts. (b) For each burst, we quantified the number of spikes and time-dependent features like latency to spike and inter-spike interval (see Section 2 for details). (c) Examples of bursts from six thalamic cells from different nuclei show different number of spikes/burst at similar hyperpolarization level prior to the burst across the cells (average − 90.92 ± 0.90 mV sd). (d) Distributions of number of spikes/burst (jittered to help visualization of individual data points) for all bursts across the population of thalamic cells in first-order (blue) and higher-order (red) nuclei. Boxes indicate the median and 25%–75% quartiles. dLGN, dorsal lateral geniculate nucleus; dMGB, dorsal medial geniculate body; LP, lateral posterior nucleus; POm, posterior medial nucleus; vMGB, ventral medial geniculate body; VP, ventral posterior nucleus [Color figure can be viewed at wileyonlinelibrary.com]
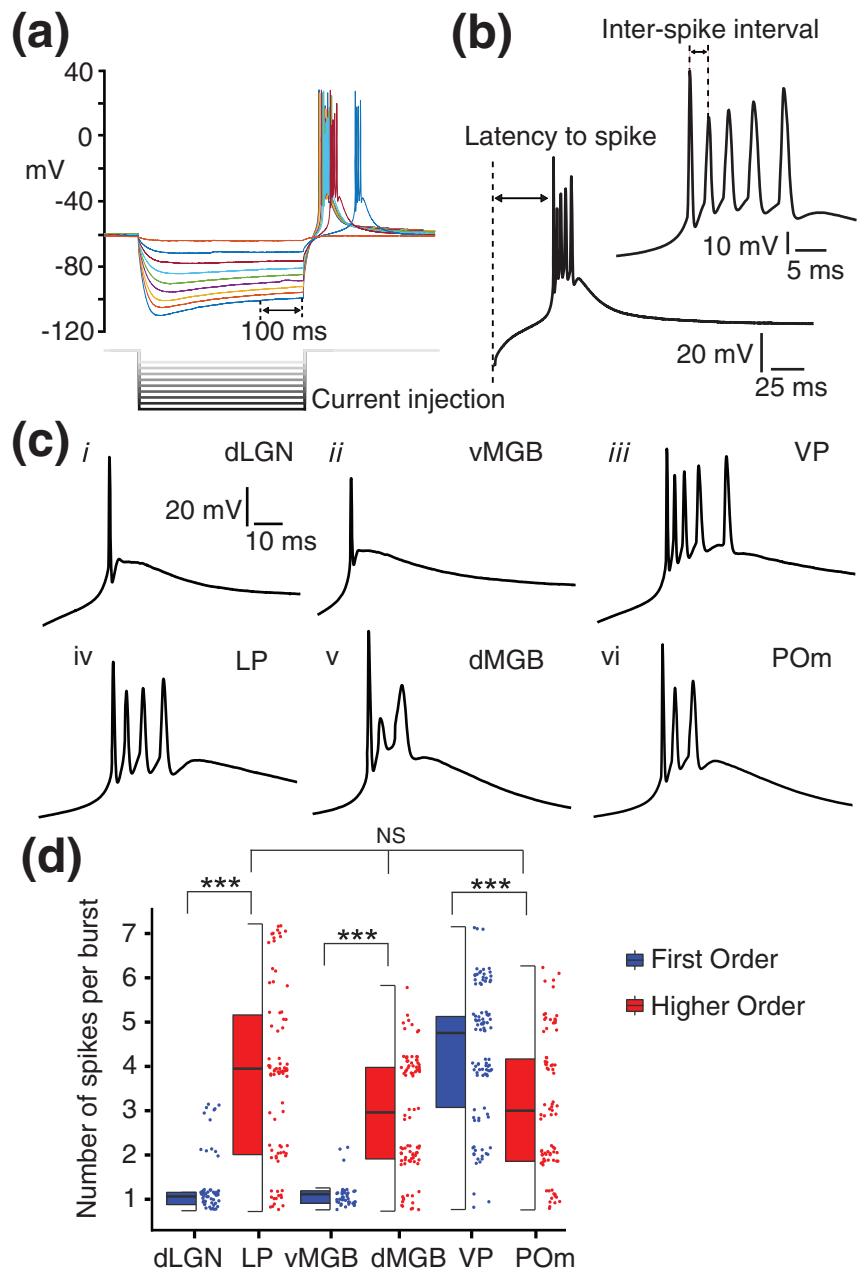
spikes after one pulse of current injection, all the other hyperpolarizing pulses induce bursts with Na$^+$-K$^+$ spikes in these cells).

When a burst occurred, it had between one and seven spikes. Figure 1(c) shows representative examples of bursts evoked in six different cells recorded in each of the six nuclei after a negative current pulse that brought the six cells to a similar hyperpolarization level. These examples show that even at similar hyperpolarization levels, cells in different nuclei produced bursts with different number of spikes. The population results (Figure 1(d); median values per nucleus in Table 1), showed that in FO nuclei, cells in the visual and auditory nuclei mostly had one spike/burst, which was significantly different from somatosensory FO cells, which had five spikes/burst on average ($p < .001$, Kruskal–Wallis test); in contrast, we did not find significant differences among the HO nuclei of different sensory systems (average LP = 4, dMGB = 3, POm = 3; $p > .27$, Kruskal–Wallis test). When

comparing FO with HO nuclei in individual sensory systems, the HO nucleus in the visual and auditory systems had more spikes/burst compared to their FO counterparts, while the FO nucleus had more spikes/burst in the somatosensory system ($p < .001$, Kruskal–Wallis test).

These results suggest that sensory HO nuclei and VP consist of cell populations that produce a broad range of spikes/burst, higher on average than in the other nuclei, and with similar distributions in HO areas (Figure 1(d)). In addition, we found that in FO nuclei the number of spikes within bursts are determined by the specific sensory system. Specifically, FO cells of the visual and auditory system produced bursts that were often limited to one spike, whereas the VP nucleus stood out from the others as having the highest proportion of bursting cells, which also produced the bursts with the highest number of spikes.

Nucleus	Sensory modality	Functional order	Number of cells (pulses)	Percent of pulses with no burst	Spikes per burst median, iqr, range	Hyperpol- arization (mV)
LGN	Visual	First	13 (87)	39	1, (1–1), (1–3)	−90 ± 14
LP	Visual	Higher	15 (107)	24	4, (2–5), (1–7)	−93 ± 14
vMGB	Auditory	First	9 (50)	14	1, (1–1), (1–2)	−83 ± 15
dMGB	Auditory	Higher	20 (128)	30	3, (2–4), (1–6)	−90 ± 14
VP	Somato-sensory	First	16 (99)	2	5, (3–5), (1–7)	−78 ± 7
POm	Somato-sensory	Higher	18 (130)	38	3, (2–4), (1–6)	−87 ± 12

Abbreviations: dLGN, dorsal lateral geniculate nucleus; dMGB, dorsal medial geniculate body; LP, lateral posterior nucleus; POm, posterior medial nucleus; vMGB, ventral medial geniculate body; VP, ventral posterior nucleus.
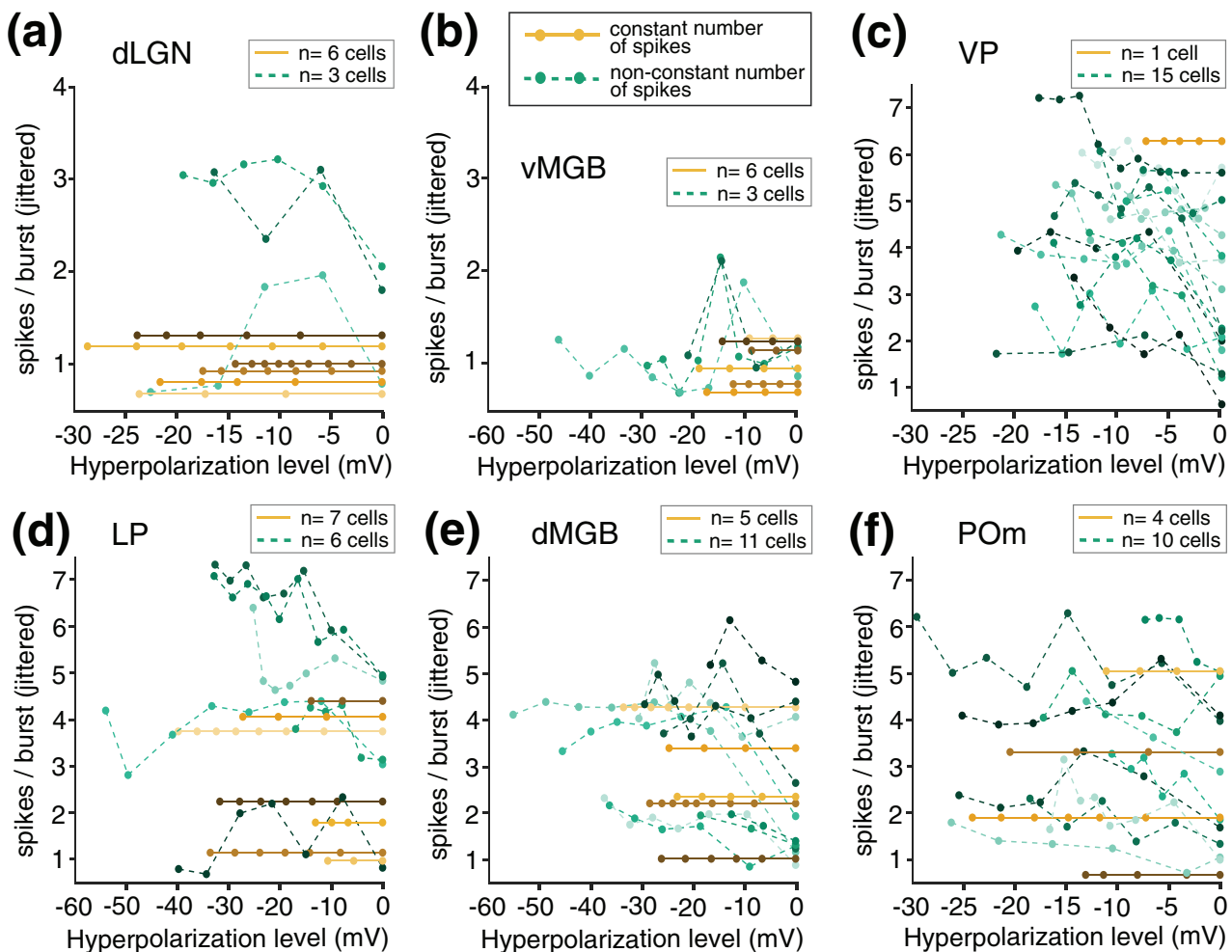

FIGURE 2 Number of spikes per burst at increasing hyperpolarization levels. Each line represents data from one cell (jittered in y-axis); zero in the x-axis corresponds to the least hyperpolarized pulse that led to a burst, and subsequent points indicate more hyperpolarized pulses with respect to this zero level. Each panel contains cells from six different nuclei (first order—(a) dLGN, (b) vMGB, (c) VP and higher order—(d) LP, (e) dMGB, (f) POm). Yellow lines represent cells for which the number of spikes per burst were constant irrespective of the hyperpolarization level, and green lines represent cells for which the number of spikes per burst varied with hyperpolarization. The number of cells in each nucleus belonging to one of the two types is included in the textbox on the top-right corner of each panel. Note that the range of the x- and y-axes was adjusted for each nucleus and is not same in all panels. dLGN, dorsal lateral geniculate nucleus; dMGB, dorsal medial geniculate body; LP, lateral posterior nucleus; POm, posterior medial nucleus; vMGB, ventral medial geniculate body; VP, ventral posterior nucleus [Color figure can be viewed at wileyonlinelibrary.com]

3.2 | The number of spikes per burst remains stable with hyperpolarization

Because the number of spikes in a burst may depend on the hyperpolarization level of the cell before the burst, we analyzed how the number of spikes per burst changed depending on the average membrane potential in a 100 ms window before the end of the current injection to the cell. Figure 2 shows the number of spikes per burst at different hyperpolarization levels for each cell in the six nuclei starting with zero referring to the least hyperpolarized trace which lead the cell to burst (yellow lines—cells with constant number of spikes and green lines—cells with varying number of spikes with hyperpolarization). For the population, we found that 38% (n = 29) of the cells that produced rebound bursts (n = 77) had a constant number of spikes regardless of the hyperpolarization level, and 62% (n = 48) showed changes in number of spikes with increased hyperpolarization. The fraction varied across nuclei, with both dLGN and vMGB being the most stable with hyperpolarization; in both dLGN and vMGB, 67% (12 out of 18 cells; Figure 2(a,b)) showed a constant number of spikes with hyperpolarization, while only 6% of cells from VP (1 out of 16 cells; Figure 2(c)) followed this trend. In the HO group (LP, dMGB, POm), a minority of cells (37%,16 out of 43 cells; Figure 2(d,e,f)) showed no change in the number of spikes with increasing hyperpolarization.

We then looked specifically at cells which showed a change in the number of spikes per burst with increasing hyperpolarization (n = 49). We compared the number of spikes produced by the first current pulse which evoked a burst in a cell, to the number of spikes produced at a higher hyperpolarization level. We found that 34 cells showed an increase in number of spikes by an average of one spike, with an average increase in hyperpolarization of 12.5 mV (from −72.83 to −85.32 mV). The remaining 15 cells did not show a consistent relationship between number of spikes and hyperpolarization, meaning that the spikes per burst went up and down with subsequent current pulses. Even in VP cells, which had the largest number of cells in which the number of spikes/burst changed with hyperpolarization, the observed changes were small (one spike on average for a hyperpolarization difference of 11.77 mV). In a subset of cells with stronger hyperpolarization (average = 22.43 mV from −73.22 to −95.65 mV, n = 22), we still found that the increase in number of spikes was one spike on average.

Lastly, to estimate the relation between spikes per burst and hyperpolarization more precisely, we used a GLM of the spikes per burst with the hyperpolarization potential as covariate; this model showed narrow and nonsignificant changes in the number of spikes with hyperpolarization (average increase in number of spikes per millivolt of hyperpolarization = 1.3% C.I. = [−8.67, 6.21], n = 49; p value = .67 Wald test). Although the confidence intervals of the GLM estimates were broad, altogether this set of results showed little change in the number of spikes with hyperpolarization in the thalamic cells we sampled. Therefore, regardless of the order or the sensory modality, the number of spikes/burst remained fairly stable for a given cell within the range of physiological membrane potential.

3.3 | Increase in within-burst spike frequency with hyperpolarization

Even if the number of spikes remains similar, the level of hyperpolarization before the pulse may influence the frequency (spike rate per second) at which the spikes in the burst occur. Figure 3(a) displays raw traces of the bursts of two sample cells at increasingly hyperpolarized membrane potentials; in one cell, the number of spikes increases with hyperpolarization and, in the other one it remains constant, but both cells show an increase in the spike rate of the first two burst spikes with hyperpolarization (Figure 3(b–e) shows all cells in LP, dMGB, VP and POm, respectively). dLGN and vMGB neurons were not included in this analysis since they mostly had one spike per burst. We compared the spike frequency of the first two spikes in the burst produced by the least hyperpolarizing current pulse, which evoked a burst in a cell (0 in panels 3(b–e)), to the spike frequency produced by at least 10 mV of additional hyperpolarization from that level for the 46 cells which had at least two spikes per burst. In this sample, 84.78% of the cells (n = 39) showed an increase in frequency by 46.4 ± 34.46 spikes/s (19.1% increase on average) from an initial frequency of 242.48 ± 64.69 spikes/s (p < .001, Wilcoxon signed-rank test) with an average increase in hyperpolarization of 12.19 mV, from −73.64 to −85.83 mV. In a subset of cells (n = 19), in which the hyperpolarization was increased further by an additional 10.44 mV, from −84.76 to −95.21 mV, the average percent increase in frequency was just 2.17% (p = .56, Wilcoxon signed-rank test). This showed that the initial increase in hyperpolarization has the largest effect on within-burst spike frequency and this effect saturates as the cell is hyperpolarized further.

Even in the group of cells which had a constant number of spikes (n = 18; yellow lines in Figure 3(a–e)) with hyperpolarization, we observed the same trend of an increase in frequency with hyperpolarization in 17 out of 18 cells; these cells showed an increase in frequency of 41.34 ± 37.17 spikes/s with an average increase in hyperpolarization of 12.85 mV (p < .001, Wilcoxon signed-rank test). Applying the GLM approach (to all cells with at least two spikes per burst; n = 46) to estimate the within-burst spike frequency with the hyperpolarization voltage as covariate, showed that the changes in spike frequency with hyperpolarization were small (average increase in frequency per millivolt of 0.75% with C.I. = [−0.2, 1.67], n = 53), but the trend was significant in 38% of the cells, with an average increase of 1.27% (p < .05, Wald test). When we looked at the within-burst spike frequency in different nuclei across all bursts with at least two spikes per burst (n = 46 cells), we did not find significant differences among any of the nuclei (p = .22, Kruskal–Wallis test; Figure 3(f)).

Lastly, for cells with at least four spikes/burst (n = 34), we quantified within-burst spike frequency adaptation as the percent change in the frequency at the last spike interval in the burst compared to the frequency at the first interval; the average within-burst spike frequency adaptation was 58.06 ± 12.46% (n = 34). When we compared the within-burst adaptation at two different hyperpolarization levels (average = −75.11 and − 85.01 mV; average difference between levels = 10.09 mV), the cells showed no significant difference in their
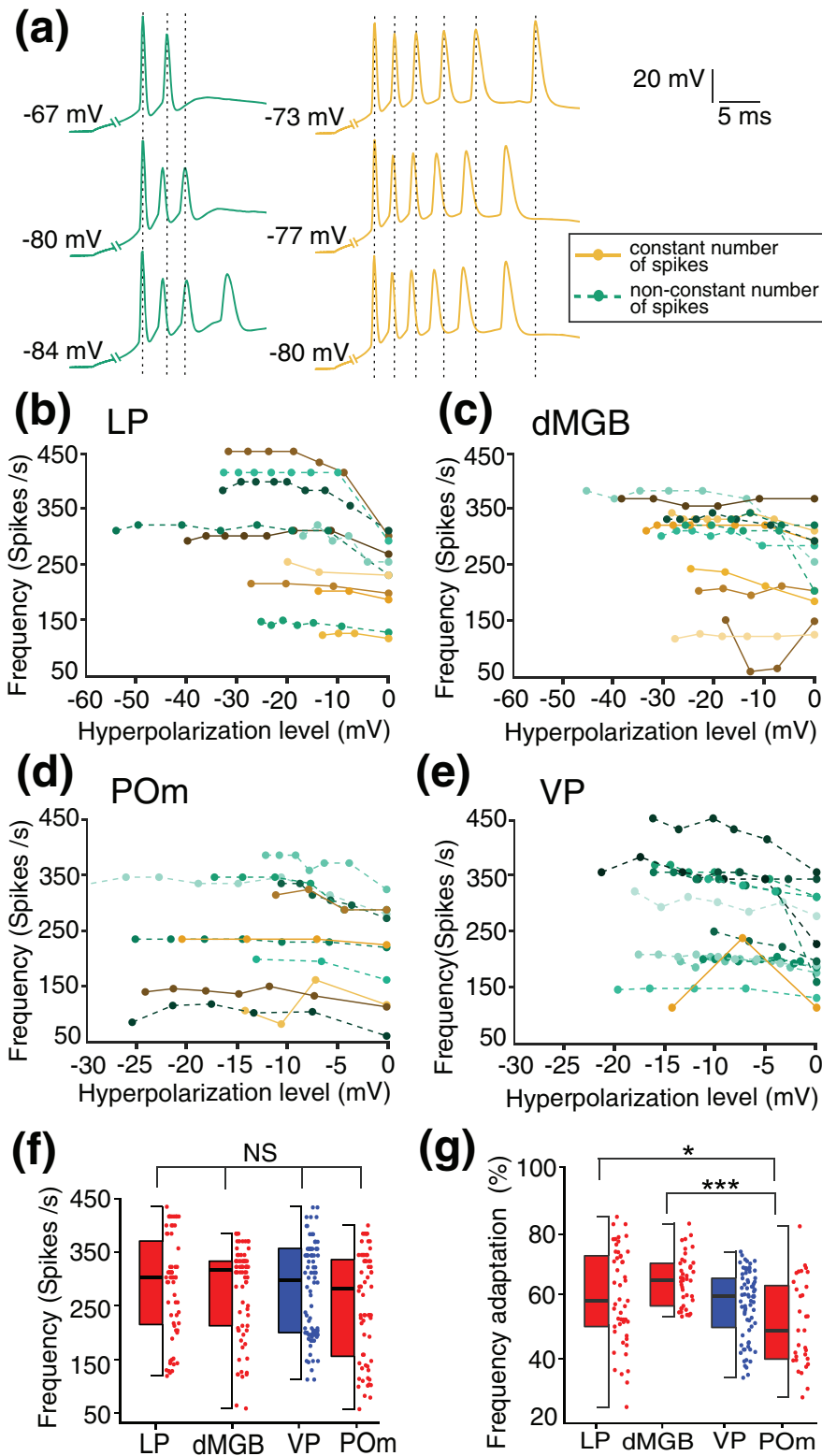
FIGURE 3 Increase in within-burst spike frequency with hyperpolarization. (a) Example bursts (from two VP cells) showing an increase in the spike rate with hyperpolarization (dotted lines), irrespective of the number of spikes per burst increasing (cell in green) or remaining constant (cell in yellow) with hyperpolarization. (b–e) Each line represents the frequency of the first intra-burst spike interval for one cell, at increasing hyperpolarization levels from the first level that produced a burst. Panels contain data for cells from four different nuclei—(b) LP, (c) dMGB, (d) POm, (e) VP. Note that the range of the x-axis is not same in all panels. (f) We found no statistical difference in the frequency across nuclei (LP, dMGB, VP and POm; dLGN and vMGB were not included in this analysis because of low number of spikes per bursts). Blue = FO; red = HO. (g) Distributions of spike frequency adaptation between last and first intra-burst intervals for cells with at least four spikes/burst show POm having lower adaptation compared to other two HO nuclei. dLGN, dorsal lateral geniculate nucleus; dMGB, dorsal medial geniculate body; LP, lateral posterior nucleus; POm, posterior medial nucleus; vMGB, ventral medial geniculate body; VP, ventral posterior nucleus [Color figure can be viewed at wileyonlinelibrary.com]

within-burst spike frequency adaptation ($p = .19$, Kruskal–Wallis test). Among HO, cells in POm had significantly lower within-burst adaptation (POm = 50.98 ± 13.6%) compared to the other two HO nuclei (Figure 3(g); LP = 59.4 ± 14.88%, dMGB = 64.16 ± 7.9%; $p < .027$, Kruskal–Wallis test).

This set of results suggests that, irrespective of the number of spikes per burst remaining constant or changing with hyperpolarization level, the spike frequency of the first ISI in a burst increases with more hyperpolarization but not the spike frequency adaptation within the burst.
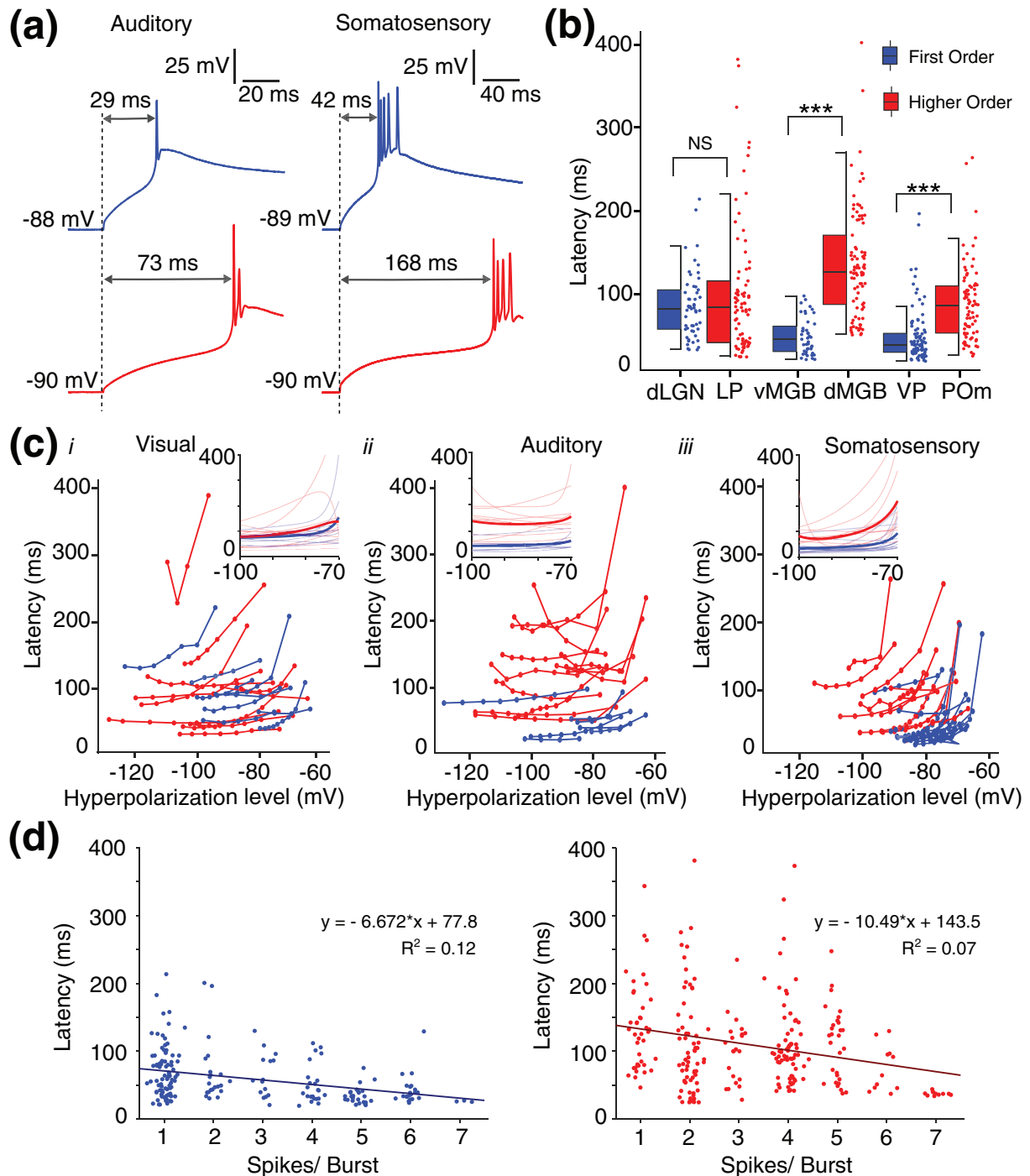
FIGURE 4 Latencies to burst reach higher values in higher-order (HO) nuclei and dorsal lateral geniculate nucleus (dLGN). (a) Bursts evoked from similar hyperpolarization levels in two cells of the auditory (left) and somatosensory (right) systems display short latency in first-order (FO) nuclei and longer latency in the corresponding HO. (b) Population distribution of the latency values for all evoked bursts. (c) Lines represent burst latencies at different hyperpolarization levels for each cell in FO (blue) and HO (red) nuclei in visual (i), auditory (ii) and somatosensory (iii) systems and show a decrease in latency with increased hyperpolarization. Insets show exponential fits for each of the cells in the raw data plots, with the average of the fits shown by darker blue and red lines (average R^2 for fits in the insets: (i) .97 ± .04, (ii) .99 ± .01, (iii) .98 ± .05). Note the difference in latencies between FO and HO at every level of hyperpolarization in auditory and somatosensory systems. (d) A negative correlation was observed in the plots of latency against number of spikes per burst for FO and HO nuclei (R^2 indicates goodness-of-fit for a linear model). Blue = FO; red = HO [Color figure can be viewed at wileyonlinelibrary.com]
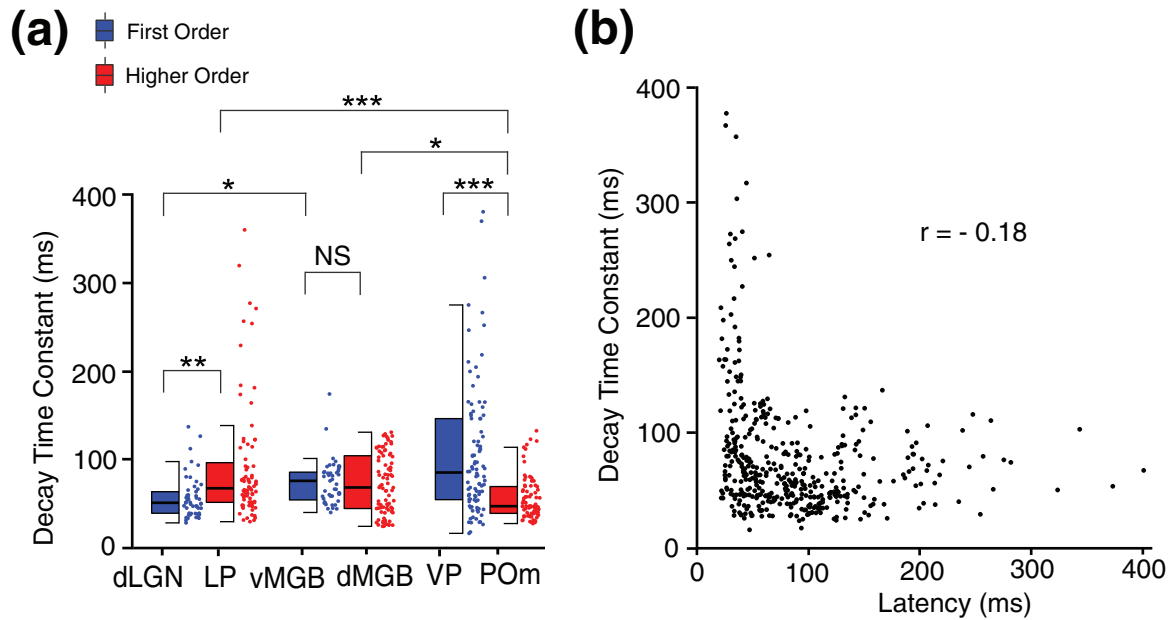
FIGURE 5 No correlation between latency and decay time constant. (a) Distribution of decay time constant across all the nuclei (see text for details). Blue = FO; red = HO. (b) No correlation between decay time constant and latency (correlation coefficient $r = -.18$) [Color figure can be viewed at wileyonlinelibrary.com]

3.4 | Longer latencies to burst in HO nuclei and dLGN neurons

The latency with which bursts are produced after hyperpolarization could influence the band-pass filter and oscillatory properties of thalamic neurons. We quantified latency as the time (in milliseconds) from the end of the current injection pulse to the peak of the first spike in the burst. Figure 4(a) shows bursts from four cells that are hyperpolarized to a similar membrane potential level (-89.25 ± 0.96 mV), and yet the vMGB and VP cells (blue traces) produced a rebound burst with much shorter latency than the dMGB and POm cells (red traces). The population data (Figure 4(b)) showed that the HO cells have significantly longer latencies than FO cells in the auditory (vMGB = 49.42 ± 21.83 ms and dMGB = 135.96 ± 64.90 ms) and somatosensory systems (VP = 48.96 ± 31.96 ms and POm = 135.96 ± 64.90 ms; $p < .001$, Kruskal–Wallis test). In the visual system, the latencies were not significantly different between the FO and HO nuclei (dLGN = 85.96 ± 39.96 ms and LP = 101.51 ± 79.35 ms; $p = .99$, Kruskal–Wallis test). Among FO nuclei, latencies in dLGN were significantly longer than vMGB and VP ($p < .001$, Kruskal–Wallis test). dMGB had the longest latencies among all nuclei ($p < .001$, Kruskal–Wallis test). The FO cells also covered a narrower range of latencies compared to HO or dLGN cells (Figure 4(b)). Even when we compared the latencies at a particular hyperpolarization (-84.83 ± 3.49 mV), we still found that FO cells in the auditory and somatosensory system had lower latencies compared to their HO counterparts (vMGB = 44.56 ± 22.37 ms and dMGB = 131.04 ± 47.88 ms; VP = 38.17 ± 22.83 ms and POm = 94.98 ± 60.97 ms, $p < .014$, Kruskal–Wallis test).

We then studied the effect of hyperpolarization on latency (Figure 4(c)). For 97% ($n = 69$) of cells, the latency decreased on average 40.72 ± 33.7 ms (from an initial value of 124.72 ± 75.74 ms) when hyperpolarized by an additional 12.63 mV from -74.02 mV ($p < .001$, Wilcoxon signed rank test). The pulses with lower hyperpolarization produced bursts with longer latency, and as the hyperpolarization increased, most cells settled into characteristic latencies. We found that the relation between hyperpolarization and latency was fitted well by a sum of two exponential functions (average goodness-of-fit $R^2 = .98 \pm .04$; exponential fits for all cells in the insets of Figure 4(c)). To test whether the latencies settle into similar values, for each cell, we used the fitted model to estimate the fastest latencies to produce a rebound burst between -70 and -100 mV of hyperpolarization. This analysis found that the shortest latency for FO cells (45.25 ± 26.84 ms) was significantly lower than the shortest latency estimated for HO cells (88.65 ± 57.72 ms, $p < .001$, Kruskal–Wallis test). These results suggest that FO and HO cells in the auditory and somatosensory thalamus differ in their rebound oscillatory properties, such that the FO cells will be able to produce rebound bursts at faster frequencies (up to about 20 Hz based on the fastest latencies estimated from the exponential model fits), whereas many HO cells may have an upper limit for rebound burst firing at about 10 Hz. Instead, the latencies we observed in the visual thalamus suggest that these cells can follow similar frequencies of bursting regardless of the order of the nucleus. We performed an additional analysis to look at the correlation between latency and the number of spikes and found a small tendency for shorter latencies to occur with more spikes per burst, and the trend was similar in FO and HO nuclei (Figure 4(d)).

Another factor that can determine the frequency of bursts in thalamocortical cells is the time that it takes for the membrane
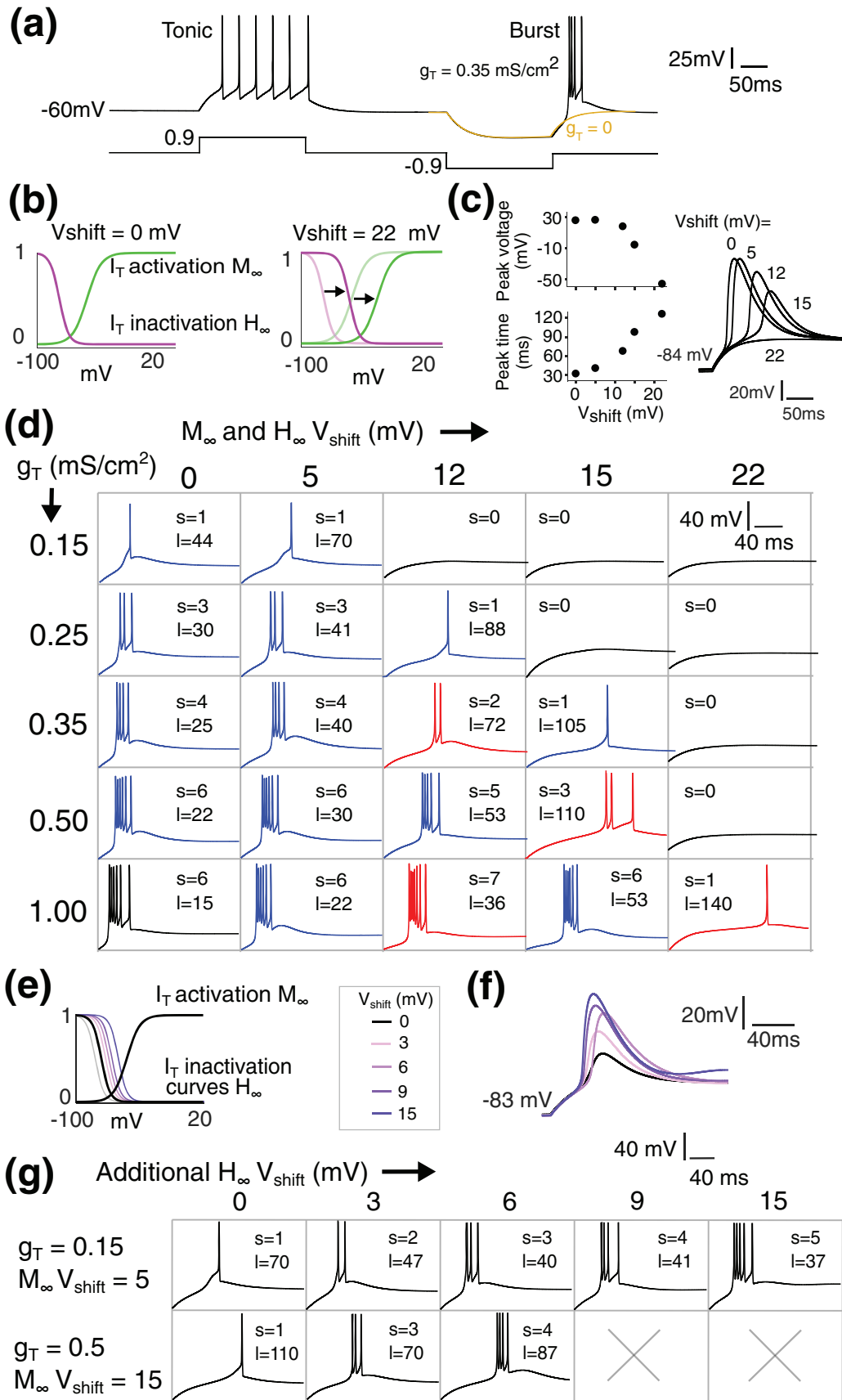
FIGURE 6 Legend on next page.

potential to decay back or recover to baseline levels after a burst. To find out whether the latency to burst was associated with different recovery times, we studied the correlation of latency with the time it took for the cell to decay back to resting membrane potential after the burst. For this analysis, we quantified the decay time constant by fitting the sum of two exponential curves to the voltage trace after the last spike in the burst ended (goodness-of-fit R^2 = .98 ± .02 for all bursts). The initial voltage drop was largely explained by the exponential function with the shortest time constant (78.82 ± 53.49 ms). When comparing cells across nuclei (Figure 5(a)), we did not find a clear association between the decay time constant and the order or sensory modality of the nucleus, and the results were more variable than the spikes/burst and latency results reported above. We found that the decay time constant was fastest for dLGN (57.08 ± 23.35 ms) and POm cells (56.76 ± 24.51 ms), followed by dMGB (72.5 ± 33.6 ms), vMGB (74.54 ± 25.44 ms), LP (92.6 ± 69.17 ms), and VP (106.16 ± 74.51 ms). In the visual system, FO cells on average had shorter decay time than HO cells (p < .01), while in the somatosensory system FO cells had longer decay time compared to HO cells (p < .001), and for auditory no significant difference was found between FO and HO cells (p = .86, all Kruskal–Wallis tests). We did not find a significant correlation between latency to burst and the decay time constant after the burst (r = −.18, Figure 5(b)), suggesting that the latency to burst and the decay back to resting membrane potential vary independently. The longer recovery times could briefly maintain thalamocortical cells above the resting membrane potential following a burst, which could switch the cell to tonic mode and delay the generation of additional bursts.

3.5 | Shifting the voltage dependence and size of the T current in a compartmental model replicates burst properties observed in different thalamic nuclei

The results on the number of spikes/burst and latencies demonstrate that bursts produced by cells in different sensory nuclei have different properties. Bursts in dLGN and vMGB had one spike on average, but the latencies in the dLGN population were significantly longer than in vMGB. On the other hand, VP cells produced higher number of spikes/burst with shorter latencies. While we saw various combinations of number of spikes and latencies in FO nuclei, HO cells showed wider ranges but more consistent distributions of burst properties across sensory systems, with an average number of spikes of 3 and latency of about 110 ms. Thalamocortical neurons in all the six nuclei we studied express the voltage-dependent CaV 3.1 T-type calcium channel. To study which properties of the T-type calcium channel can account for bursts with different combinations of number of spikes and latencies, we implemented a single compartment model of a thalamocortical cell using the DynaSim simulation environment (Benita et al., 2012; Sherfey et al., 2018; Soplata et al., 2017; see Section 2 for details). The model replicates the tonic and burst firing properties of thalamocortical neurons (Figure 6(a)) and it allowed us to investigate the properties of the T current that may contribute to different bursts.

Experimental evidence suggests that the voltage dependence of the T channels varies across thalamic cells. For example, the voltage at which half of the T current is activated can range between −45 and −60 mV even among cells of the same nucleus (Huguenard, 1996; Perez-Reyes, 2003). The voltage dependence of the activation and inactivation curves of thalamic ion channels has important functional implications because it is regulated by spike activity (Cazade et al., 2017), neuromodulators (McCormick & Williamson, 1991; Pape, 1992), and antipsychotics (Perez-Reyes, 2003). In addition, the overall size of T-type conductance can be regulated irrespective of kinetics, for example, through changes in channel density (Chung et al., 1993; Perez-Reyes, 2003; Tsakiridou et al., 1995). Therefore, we investigated whether changes in the voltage dependence of the T current and in the size of the conductance were sufficient to evoke burst properties like those we observed in the data.

We systematically shifted the activation M_∞ and inactivation H_∞ curves of the T current to more depolarized values up to 20 mV (Figure 6(b)), based on the experimental evidence (Huguenard, 1996; Perez-Reyes, 2003) and because this range of membrane potentials is critical for switching between burst and tonic firing modes. Shifting the curves reduced and delayed the amount of T current produced at a given membrane potential (Figure 6(c)). We then tested different combinations of V_{shift} (Figure 6(d), columns) with increasing values of T-channel conductance (g_T; Figure 6(d), rows). For a fixed value of g_T, increasing the shift led to longer latencies and a reduction in the number of spikes. As we increased g_T for a given value of V_{shift}, we

---

FIGURE 6 T current kinetics replicate burst properties of first-order (FO) and higher-order (HO) neurons. (a) Compartmental model of a thalamocortical cell reproduces tonic and burst modes of response (yellow trace after removing the T current). (b) Activation (green) and inactivation (magenta) curves used in the model were shifted in the x-axis (voltage dependence) to test their effect on burst properties. (c) T current evoked after hyperpolarization to −84 mV at different values of V_{shift}; note the decrease in amplitude and longer delay in the T current peak with larger shifts. (d) Burst results obtained with different combinations of V_{shift} values (columns) and different maximum T conductance values (rows). The color code indicates simulations that replicate bursts observed in FO (blue) and HO (red) cells. s = spikes/burst; l = latency. (e) Shifting the inactivation curve to a more hyperpolarized level (gray line) led to no burst. Other curves represent the inactivation curve shifted to a more depolarized level. V_{shift} values represent the additional amount by which inactivation curves are shifted compared to the activation curve. (f) T current evoked after hyperpolarizing the model to −83 mV when the inactivation curve was shifted by different amounts; note the increase in amplitude with larger shifts. (g) Simulation results for a particular g_T and M_∞: V_{shift} showed that increasing the relative $H_\infty V_{shift}$ led to an increase in spikes/burst. Only the initial shifts in H_∞ led to a decrease in latency. s = spikes/burst; l = latency [Color figure can be viewed at wileyonlinelibrary.com]

observed a decrease in latency and an increase in number of spikes. Figure 6(d) shows the effect of different combinations of V_{shift} and g_T with the model cell being hyperpolarized to -85.53 ± 0.80 mV. For each simulated burst, we calculated the probability of obtaining a burst with the same number of spikes and latency in each of the six nuclei based on the probability distributions from the in vitro data (see Section 2, Figures 1(d) and 4(b)). This allowed us to identify whether the simulated burst was most likely to be produced by a FO or HO nuclei (indicated by blue or red in Figure 6(d)). We found that lower values of V_{shift} (<12 mV) produced bursts consistently similar to those in FO nuclei. In addition, models with the highest g_T (0.35–1 mS/cm^2) and shifts (V_{shift} = 12–22 mV) produced bursts with longer latencies and a greater number of spikes, which were more likely to correspond to HO properties. These results put forward the hypothesis that differences in the number of spikes/burst and latencies observed in bursts of FO and HO nuclei, may be caused by differences in the voltage dependence of the activation and inactivation curves and the total conductance of T-type channels expressed in thalamocortical neurons.

We then changed the relative position between the activation and inactivation curves and tested the effect on the T current (Figure 6(e)). Moving the inactivation curve toward more hyperpolarized potentials did not lead to bursts; shifting it to more depolarized potentials, led to an increased amount of T current and an increase in the spikes/burst (Figure 6(f,g)). This suggests that even if the total T-channel conductance for a cell were constant, it may produce bursts with different number of spikes in conditions that modulate the relative voltage dependence of the activation and inactivation curves.

3.6 | The diversity of spikes per burst and latency to burst is not explained by intrinsic properties or rat age

We found that the number of spikes per burst and latency (but not the within-burst spike rate) vary according to the nucleus order and sensory modality and may be explained by changes in the voltage dependence and conductance of T channels. We considered if the variation in burst properties could be explained by cellular passive properties (membrane capacitance [Cm] and membrane resistance [Rm]) or by age in a random sample of cells in which the three properties (Cm, Rm, age) were recorded (n = 61; 67% of the full sample). Burst properties in rodents develop during the first postnatal days and are similar to the adult by age P12-13 (Perez Velazquez & Carlen, 1996; Ramoa & McCormick, 1994; Tennigkeit et al., 1998; Warren & Jones, 1997). We found no significant age differences among cells in different nuclei (n = 61; p > .4, Kruskal–Wallis; Figure 7 (a); Table 2). However, we found that in LP (but not in POm, dMGB or in the FO nuclei) there was a significant negative correlation between age and latency to the first spike in the burst (r = −.77; n = 11; p = .03), suggesting that in LP the latency to burst may be under developmental control and decrease with age. The membrane
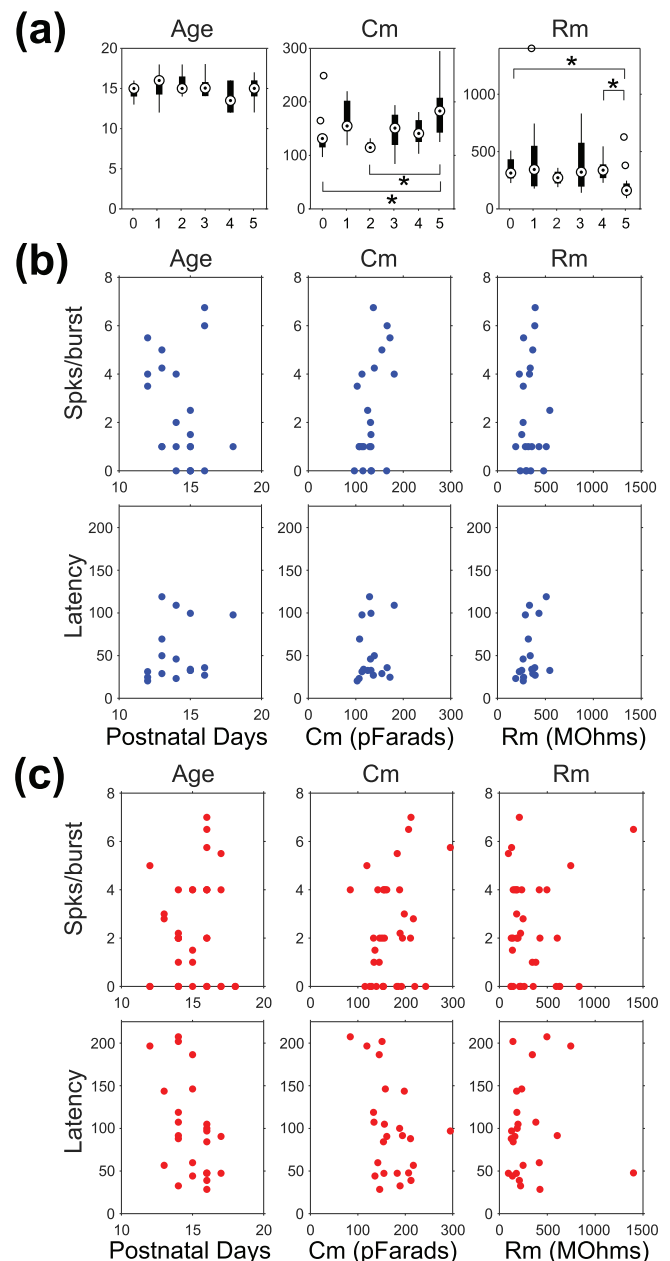

FIGURE 7 Intrinsic properties and age in first-order (FO) and higher-order (HO) neurons. (a) Population distributions of age (postnatal days), membrane capacitance (Cm, in picoFarads) and membrane resistance (Rm, in MegaOhms); 0 = dLGN, 1 = LP, 2 = vMGB, 3 = dMGB, 4 = VP, 5 = POm. (b) Age (left), membrane capacitance (middle) and membrane resistance (right) in relation to the number of spikes per burst and the latency for FO cells (in all plots, each dot represents data from one cell). (c) Same for HO cells. dLGN, dorsal lateral geniculate nucleus; dMGB, dorsal medial geniculate body; LP, lateral posterior nucleus; POm, posterior medial nucleus; vMGB, ventral medial geniculate body; VP, ventral posterior nucleus [Color figure can be viewed at wileyonlinelibrary.com]

capacitance was significantly larger in POm compared to dLGN and to vMGB neurons, while POm neurons had lower membrane resistance compared to dLGN and VP (p = .03; Kruskal–Wallis; Figure 7(a)). While a larger membrane capacitance may reflect larger cell size in

Nucleus (number of cells)	Post-natal age (days)	Cm (pF)	Membrane resistance (MOhms)
LGN (10)	15 ± 1	140 ± 43	342 ± 100
LP (11)	15 ± 2	166 ± 35	439 ± 368
vMGB (4)	16 ± 2	117 ± 11	273 ± 70
dMGB (11)	15 ± 1	147 ± 35	387 ± 229
VP (10)	14 ± 2	143 ± 25	339 ± 94
POm (15)	15 ± 2	182 ± 47	209 ± 136

TABLE 2 Average rat age, neuronal passive properties (Capacitance, Cm, and membrane resistance) in a random sample of 61 cells (values are mean ± *SD* in each nucleus)

Abbreviations: dLGN, dorsal lateral geniculate nucleus; dMGB, dorsal medial geniculate body; LP, lateral posterior nucleus; POm, posterior medial nucleus; vMGB, ventral medial geniculate body; VP, ventral posterior nucleus.

POm, and larger cells may contain proportionally more T channels, the additional T current would distribute over a larger area and it is unlikely to produce by itself an increased number of spikes per burst in POm.

We did not find significant correlations between burst latency and membrane capacitance or membrane resistance in any of the nuclei ($p > .05$), nor between the number of spikes per burst and age, capacitance or membrane resistance in any of the nuclei ($p > .16$, Kruskal–Wallis; Figure 7(b) for FO and 7(c) for HO). These analyses suggest that age or the membrane passive properties do not explain the different burst properties across nuclei, although age may be an important factor in regulating the latency to burst in LP neurons.

In addition to passive properties, several intrinsic conductances influence the tonic and burst firing of thalamic neurons (Amarillo et al., 2014; Llinás, 2014; Sherman & Guillery, 2001). In particular, I_h works in coordination with the T current to determine oscillatory firing in thalamic cells (Lüthi & McCormick, 1998; McCormick & Pape, 1990). I_h is a mixed cation current responsible for a "sag" in the voltage in response to a steady hyperpolarizing current, and it is possible that the I_h evoked by the hyperpolarizing pulses could influence the number of spikes or latency in the subsequent rebound burst. To investigate potential differences due to I_h, we quantified the sag voltage (Figure 8(a)) during the hyperpolarization pulses (for all pulses that produced a burst; $n = 77$ cells) by calculating the difference between the minimum membrane voltage at the start of the hyperpolarization pulse (≤ 125 ms) and at 250 ms after that minimum, based on the activation dynamics of I_h (McCormick & Pape, 1990). We obtained the sag voltage for each cell as the average sag in pulses that hyperpolarized the cell to a voltage between −85 and −95 mV. We found significant differences in the sag values among FO and HO cells in the auditory system (Figure 8(b), vMGB = 5.55 ± 1.81 mV and dMGB = 1.20 ± 1.11 mV, $p < .001$, Kruskal–Wallis test) but no significant difference in the sag values among FO and HO cells in visual and somatosensory nuclei (Figure 8(b), LGN = 1.79 ± 0.94 mV and LP = 2.94 ± 1.99 mV, $p = .92$, Kruskal–Wallis test; VP = 3.95 ± 2.33 mV and POm = 5.25 ± 3.58 mV, $p = .98$, Kruskal–Wallis test; $n = 64$). Cells with no sag (in which the voltage became progressively more negative in the 250 ms window; Figure 8(a) green trace) were removed from this analysis. dMGB had the highest percent of cells with no sag in the hyperpolarization range of −85 mV to

−95 mV (LGN = 12.5%, vMGB = 11.11%, VP = 0%, LP = 16.67%, dMGB = 26.67%, POm = 7.69%).

We then asked if having a strong sag influences the properties of the subsequent rebound burst after the current injection ends (Figure 8(c–f)). For each cell with a positive sag value, we compared the sag voltage with the number of spikes per burst and latency for pulses that produced a hyperpolarization between −75 and −85 mV right before the end of the current injection ($n = 70$ cells). We found no significant correlation between sag voltage and the number of spikes per burst (Figure 8(c) for FO and 8(e) for HO); however, there was a trend for the shortest latencies to occur in cells with highest values of sag voltage, which was similar in FO and HO (Figure 8(d) for FO and 8(f) for HO), even though there was no significant difference in the membrane potential of the cells right before the burst was evoked ($p > .19$, Kruskal–Wallis test). The significant difference in sag voltage between vMGB and dMGB and the inverse relationship between sag voltage and latency might contribute to the shorter latencies we observed in vMGB compared to dMGB (shown in Figure 4(b,c)). On the other hand, sag values do not seem to explain the differences in burst properties in somatosensory and visual FO and HO nuclei. These results suggest that I_h does not determine the different burst properties that we found in FO and HO nuclei, but it may have a general role in reducing the latency to burst in thalamic neurons.

Another current that might affect burst properties is the depolarization-activated K$^+$ (I_A) current. We did not assess the role of I_A in our in vitro recordings; nonetheless, to gain insight on the relationship between the I_A current and burst properties, we used our single compartment thalamic model and added the I_A current used in the study by Benita et al. (2012). We systematically varied the A channel conductance from 0 to 5 mS/cm^2 (McCormick & Huguenard, 1992; Rush & Rinzel, 1995). g_T and V_{shift} were kept constant in this model at 1 mS/cm^2 and 0 mV. The results (Figure 8 (g,h)) show an inverse relation between the number of spikes per burst and g_A where the number of spikes decreased from 11 to 1, and a positive correlation between g_A and latency (which increased with g_A from 15 to 40 ms). While the role of I_A needs to be studied in further experimental detail, these simulations are consistent with previous models (Amarillo et al., 2014; McCormick & Huguenard, 1992; Rush & Rinzel, 1995) and suggest that I_A could
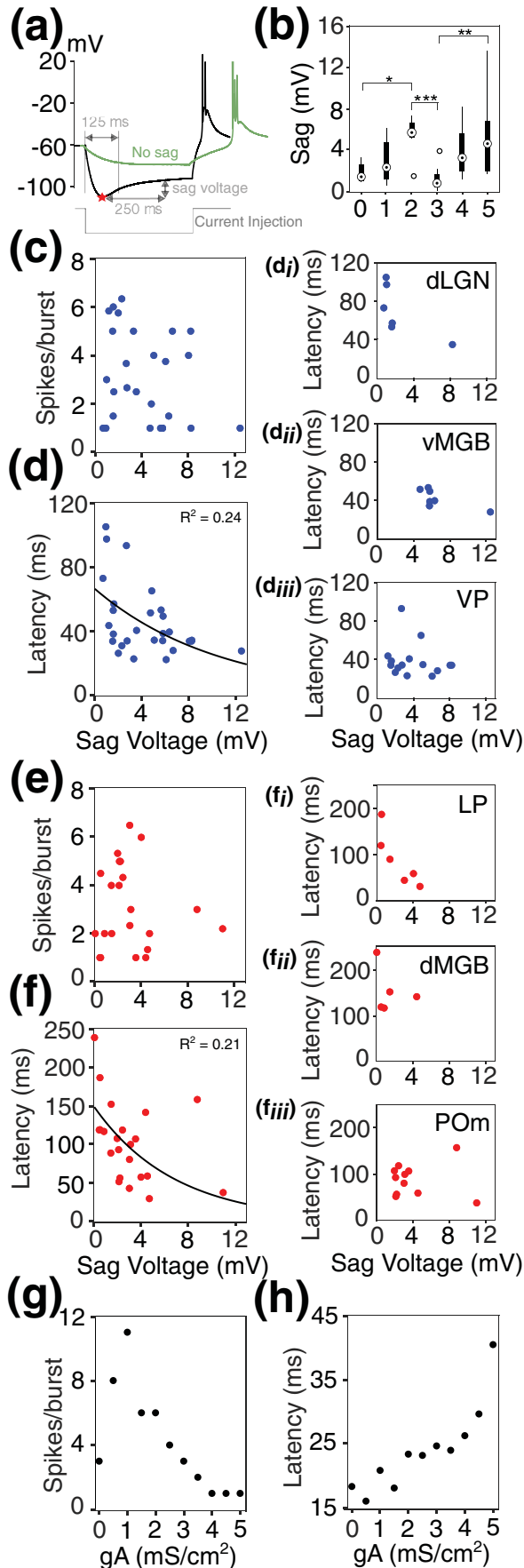
contribute to regulate burst properties by reducing the number of spikes/burst and slowing burst latency.

3.7 | Functional implications of different burst properties: Release probability and thalamocortical transmission

Bursts have been suggested to be more effective at activating post-synaptic cortical cells than tonic firing because of the multiple spikes and the quiescent period preceding the burst (Hu & Agmon, 2016; Swadlow & Gusev, 2001). Driver thalamocortical synapses have high-release probability and a slow recovery time constant to replenish synaptic vesicles in the presynaptic terminal, which may undermine the effectiveness of subsequent bursts. Each spike in a burst would reduce the probability of neurotransmitter release, decreasing the effectiveness of upcoming spikes in the same burst and from subsequent bursts. On the other hand, having a long latency leading to burst spikes may allow for the presynaptic terminal to recover. Using simulations, we studied the combined effect of the number of spikes per burst and burst latency on the release probability at a thalamocortical synaptic terminal. In each simulation, the thalamic cell model was made to spike with the same number of spikes and intraburst dynamics as found in the in vitro data (example in Figure 9 (a)). This was achieved by applying a brief 2 ms current pulse to the model which produced one spike, and the pulse was repeated at intervals corresponding to the inter-spike intervals within a burst. We then made the thalamic cell produce another burst after at least 100 ms (to provide enough time for the T channels to completely de-inactivate). We quantified the release probability (Section 2) that the first

FIGURE 8 Sag voltage does not explain the diversity of burst properties and correlates with latency in both first-order (FO) and higher-order (HO) nuclei. (a) The sag voltage was quantified by calculating the difference between the minimum membrane voltage at the start of the hyperpolarization pulse ($\leq$125 ms) and at 250 ms after that minimum. Green trace is an example of no sag. (b) Distributions of sag voltages (in pulses between -85 and -95 mV in the initial 125 ms of current injection) compared across the six nuclei. 0 = dLGN, 1 = LP, 2 = vMGB, 3 = dMGB, 4 = VP, 5 = POm. (c) Number of spikes per burst versus sag voltages for FO cells shows no correlation between the two quantities. (d) Latency versus sag voltages in FO cells shows an inverse correlation; black line is an exponential fit. (di,ii,iii) show the correlation between sag and latency for the individual nuclei. Sag for burst properties analyses was calculated from pulses with similar hyperpolarization immediately before the burst (-75 to -85 mV). Cells with no sag are not shown in the plots. (e) and (f) same as (c) and (d) for HO nuclei. (g, h) Simulations in the compartmental thalamic model showed that increasing g_A led to a decrease in the number of spikes/burst (g) and to an increase in latency (h). dLGN, dorsal lateral geniculate nucleus; dMGB, dorsal medial geniculate body; LP, lateral posterior nucleus; POm, posterior medial nucleus; vMGB, ventral medial geniculate body; VP, ventral posterior nucleus [Color figure can be viewed at wileyonlinelibrary.com]
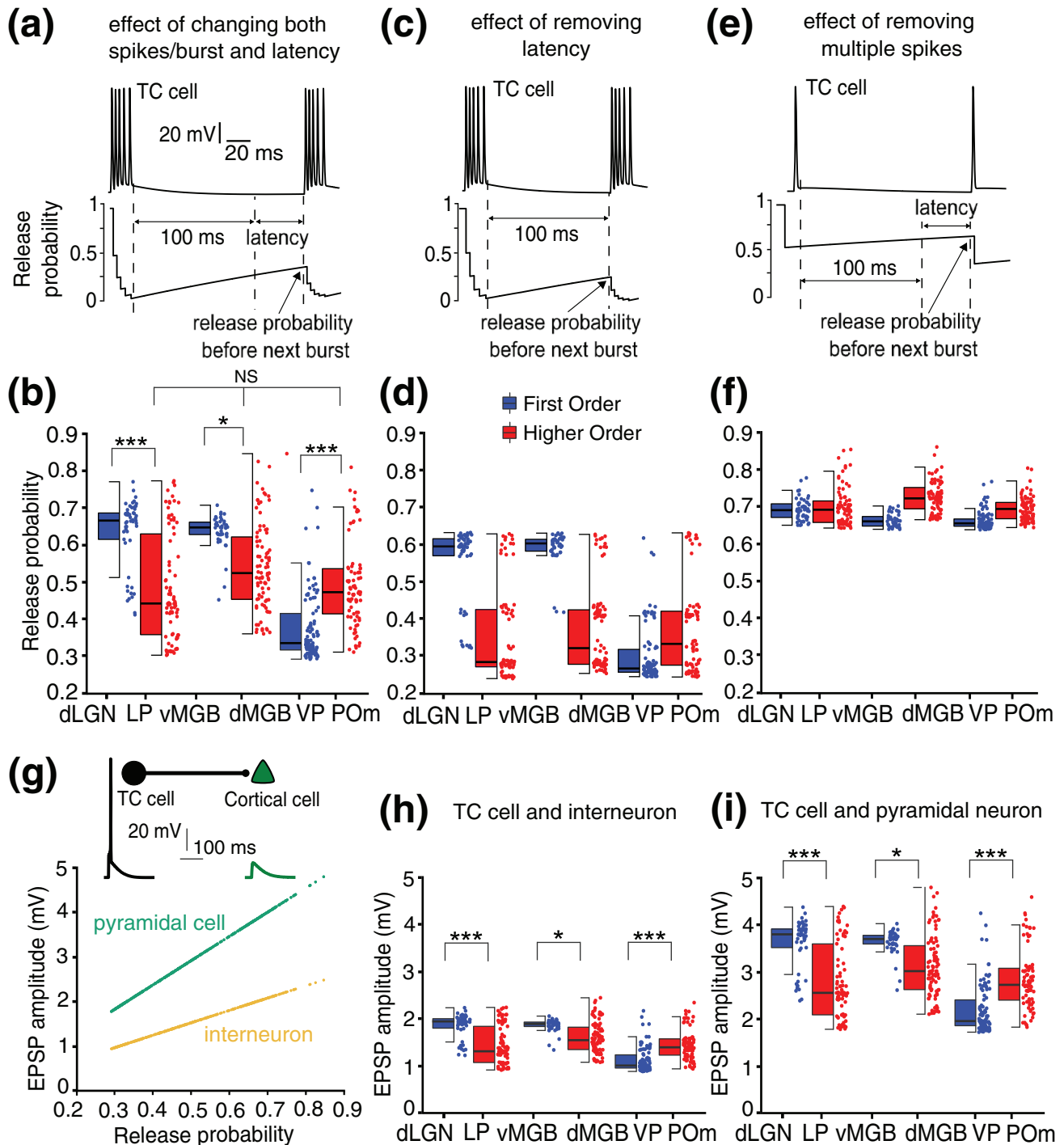
FIGURE 9 Number of spikes per burst significantly reduces the probability of release at thalamocortical terminals. (a) Example simulation showing the release probability over time after a burst that mimics the features obtained from a recorded thalamocortical (TC) cell; release probability values were obtained at the time indicated by the arrow (following 100 ms plus the latency obtained from all evoked bursts). (b) Distribution of release probabilities obtained after simulations that mimic spikes per burst and latencies in all recorded nuclei. (c, d) Distribution of release probabilities using only the values of spikes per burst (release probability estimated at 100 ms). (e, f) Distribution of release probabilities using only latency values from the in vitro data and after a burst with only one spike. Blue = FO; red = HO. (g) Linear correlation between excitatory postsynaptic potential (EPSP) amplitude and the synapse's release probability from simulations in a thalamocortical model that contacts a pyramidal cell (green) or an interneuron (yellow). (h, i) Effect of a TC spike on EPSP amplitude (mV) in two types of cortical cells (interneuron and pyramidal) simulated at different synaptic release probabilities observed in the simulations in (b) [Color figure can be viewed at wileyonlinelibrary.com]

spike in this burst would encounter, that is, the release probability at 100 ms plus the burst latency of each of the recorded cells.

First, we considered the combined effect of both the number of spikes and latency from each cell on release probability (Figure 9(a,b)). We found that bursts with the properties of HO nuclei neurons led to similar values of release probability irrespective of the sensory system (0.51 ± 0.13; p > .05, Kruskal–Wallis test). Bursts like those seen in FO visual and auditory systems depleted the thalamocortical terminal less than the HO bursts (FO = 0.63 ± 0.08, HO = 0.52 ± 0.13, p < .029, Kruskal–Wallis test). This suggests that bursts from a neuron in dLGN or vMGB might be more effective in propagating information to their postsynaptic cells in cortex. This was not the case in the somatosensory system, and we found that VP bursts led to the most depleted terminals and the lowest release probabilities (VP = 0.38 ± 0.09, POm = 0.49 ± 0.11, p < .001, Kruskal–Wallis test). Second, we removed the effect of latency by quantifying release probability at a fixed time of 100 ms after the first burst ends (Figure 9(c,d)). When the effect of latency was removed, the probability of release decreased in all nuclei compared to the previous test (due to the second burst being evoked earlier), and the percent decrease in release probability was higher in nuclei that have the largest number of spikes per burst, that is, HO and VP (decrease with respect to Figure 9(b): LP = 26.9%; dMGB = 28.28%; POm = 24.8%; dLGN = 13.75%; vMGB = 7.25%; VP = 20.15%, p < .001, Wilcoxon signed-rank test), suggesting that latency is an important factor to facilitate thalamocortical transmission in cells with higher spikes/ burst. Lastly, we removed the effect of multiple spikes by making the thalamocortical model neuron fire only one spike and calculating release probability after latency (Figure 9(e,f)). This increased the release probability for all the nuclei (p < .001, Wilcoxon signed rank test), but more dramatically in nuclei with higher spikes/burst (increase with respect to Figure 9(b): LP = 53.3%; dMGB = 35.05%; VP = 82.79%; POm = 47.08%) compared to dLGN = 11.75% and vMGB = 4.78%. Notably, the distributions became very compact,

suggesting that most of the variance in release probability is due to the depressing effect of high numbers of spikes/burst. This set of results suggests that release probability is highly dependent on the spikes/burst, and that latency can play a significant role to recover synaptic release properties in nuclei with higher numbers of spikes per burst, such as for all the HO nuclei we studied and VP.

We then extended this analysis to study how different release probabilities due to a burst may affect the effectiveness of a subsequent thalamic spike on cortical cells. For these simulations, we used a model of a thalamic neuron connected to a cortical interneuron or to a pyramidal cell (Benita et al., 2012). The synapse's release probability was set to the values obtained from the previous simulations (Figure 9(b)), which combined the effect of different number of spikes per burst and latencies from our in vitro burst data. We then made the thalamic cell produce a spike by applying a 2 ms pulse of positive current. We quantified the effect of the thalamocortical spike on the cortical cell as the size of the EPSP (mV) from the resting potential of the cortical cell. The simulation results showed a linear relationship between the cortical cell EPSP and release probability (Figure 9(g)). These results suggest that the differences in burst properties among FO and HO nuclei in all the three sensory systems would lead to a significant difference in the amplitude of EPSPs evoked in cortical cells (interneuron = Figure 9(h), pyramidal cell = Figure 9(i)). A spike following a burst from HO thalamic nuclei would lead to similar EPSP amplitudes in cortical cells across different sensory modalities (interneuron [IN]= 1.50 ± 0.36 mV, p > .05, pyramidal (PyC) = 2.93 ± 0.71 mV, p > .05, Kruskal–Wallis test). dLGN and vMGB would have the least depressed synapse, leading to the largest EPSP as a result of spikes following a burst (dLGN: IN = 1.85 ± 0.26 mV, PyC = 3.62 ± 0.52 mV, p < .01; vMGB: IN = 1.86 ± 0.13 mV, PyC = 3.63 ± 0.26 mV, p < .05, Kruskal–Wallis test). Bursts from VP would keep the synapse most depressed among the six nuclei we studied, leading to the smallest EPSPs (IN = 1.12 ± 0.26 mV, PyC = 2.2 ± 0.51 mV, p < .001, Kruskal–Wallis test).
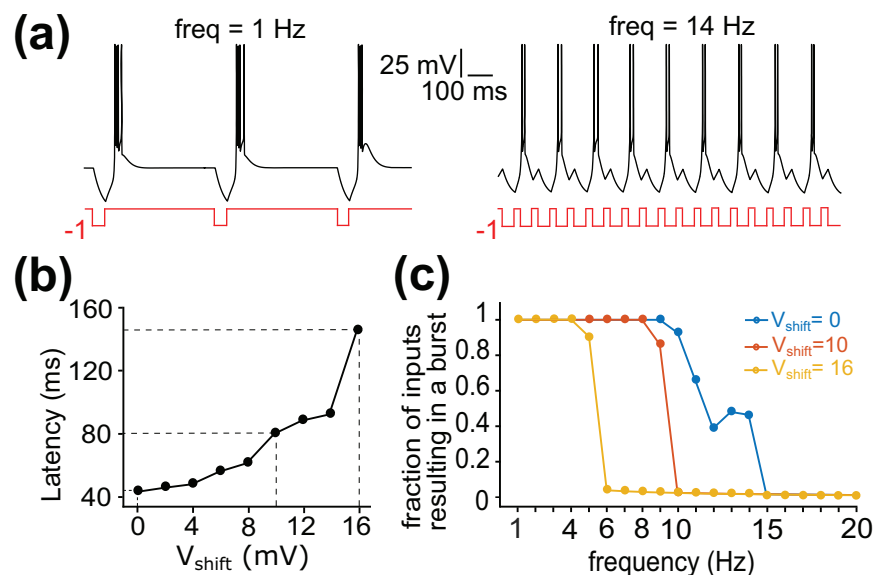

FIGURE 10 Latency to burst sets a cutoff frequency for rebound bursting in thalamic neurons. (a) Example simulation in which the TC model cell receives 50 ms negative current pulses at 1 Hz (left) or 14 Hz (right). (b) Latency values obtained at progressively larger V_{shift}. Dashed lines indicate the values selected for the simulations in (c). (c) Fraction of inhibitory pulses applied at increasing frequencies that result in a burst; increasing V_{shift} values (color coded) result in progressively lower cutoff frequencies [Color figure can be viewed at wileyonlinelibrary.com]

3.8 | Longer burst latencies determine slower rebound burst frequencies in thalamocortical neurons

Thalamocortical cells fire rebound bursts in response to inhibitory input from the thalamic reticular nucleus (TRN), which fires bursts at frequencies of 7–15 Hz (Bal & McCormick, 1993; Fuentealba & Steriade, 2005), or other sources of inhibition such as the zona incerta (Barthó et al., 2002; Halassa & Acsády, 2016). As we found bursts with latencies ranging from 19 ms to 400 ms (average 87.75 ms for the cell population), neurons with the longer latencies may not be able to burst in response to high frequency inhibitory input. This would mean that burst latency sets an upper limit on the frequency of the input that a thalamocortical neuron is able to keep up with.

To find this upper limit in the model, we applied brief (50 ms) hyperpolarizing pulses to the model cell at different frequencies (Figure 10(a)) and measured the fraction of inhibitory inputs for which the cell produced a burst. We simulated the cell with a fixed g_T ($g_T = 1$ mS/cm^2) and with different burst latencies (43, 80, and 145 ms, by setting V_{shift}, respectively, to 0, 10, and 16 mV, Figure 10(b)). In Figure 10(c), we can observe that for $V_{shift} = 0$ mV, which represents cells with shorter latencies, the model cell is able to respond with a burst to almost 100% of the inputs up to 10 Hz, after which the fraction of pulses that induce a burst goes down to 40% at 14 Hz, and the model is not able to respond to inputs beyond 15 Hz. For $V_{shift} = 10$ mV, the cells are not able to burst with frequencies beyond 10 Hz and for $V_{shift} = 16$ Hz this limit reduces to 6 Hz. Interestingly, for cells with larger V_{shift} the drop in response from 100% to 0% is sudden, occurring within 2 Hz, while for $V_{shift} = 0$ the response drops gradually in 6 Hz.

These simulations show that cells with short latencies can completely or partially keep up with hyperpolarizing input of frequencies up to about 15 Hz. vMGB and VP had the shortest latencies (49.1 ± 29.14 ms), suggesting that these cells might be able to keep up with frequencies of up to 15–20 Hz. Latencies for cells in dLGN, LP, and POm averaged 92.98 ± 59.76 ms, which might put an upper cap on the rebound bursting frequency at 10 Hz. That said, these cells had a wide range of latencies, and 25% of them showed latencies less than 50 ms, which suggest that some of cells would be able to keep up with faster frequencies. For dMGB, which had the longest latencies (135.94 ± 64.9 ms), the simulations suggest that these cells might not be able to follow inputs with frequencies higher than 6 Hz. Overall, the voltage-dependent properties of the T current may provide an intrinsic mechanism that limits the oscillatory frequency of rebound bursting in thalamic cells.

4 | DISCUSSION

We used whole-cell intracellular recordings of rebound bursts in six sensory thalamic nuclei to determine whether there are burst features that are linked to the hierarchical order of a nucleus (FO or HO) or to specific sensory modalities (visual, somatosensory, and auditory). In the nuclei that we studied, we found that burst properties overlapped

in their distributions but were significantly different in some nuclei. Both the order (FO or HO) and the sensory modality determined the burst properties of neurons. Individual FO nuclei were quite distinct, neurons in the vMGB had the narrowest range of feature distributions compared to all the other nuclei, displaying few spikes per burst and short latencies; dLGN bursts were characterized by few spikes and longer latencies, and VP had short latencies and a high number of spikes per burst. Cells in HO nuclei had burst properties that overlapped with those of FO neurons, but the three HO nuclei were consistent in that they had higher values of average number of spikes per burst (similar to VP) and longer latencies to the first spike (like dLGN). A compartmental model showed that changes in the voltage dependence and density of the T-channel conductance are sufficient to generate the diverse burst features observed in the intracellular data. Lastly, we studied the implications of different types of bursts for transmission in the thalamocortical synapse and for rhythmic bursting in thalamic cells. We found that model neurons with low numbers of spikes per burst preserved a more effective thalamocortical synapse for a spike following the burst. In addition, in bursts with more spikes, the latency played a role in facilitating the probability of release and transmission at the thalamocortical synapse by a subsequent spike. We found that long latencies can also limit rhythmic rebound bursting to about 15 Hz in FO and 6 Hz in HO cells. In summary, the results suggest that although bursts are fairly stereotypical, the number of spikes per burst and latency to the first spike depend on the sensory modality and order of thalamic neurons, and these burst features will determine the effectiveness of thalamocortical transmission and the oscillatory properties across thalamic nuclei.

4.1 | Burst properties and the functional organization of thalamocortical networks

In addition to the type of information being processed, the architecture of long-range input and output connections is key to understanding the function of thalamocortical cells within the forebrain. FO nuclei occupy an early position in their sensory systems and receive their primary input from noncortical regions, whereas HO thalamocortical cells receive driver input that has already been processed by cortex and are more deeply embedded in cortical networks (Bickford, 2015; Clascá et al., 2012; Guillery & Sherman, 2002; Phillips et al., 2019; Rovó et al., 2012; Sherman & Guillery, 2011). Our analyses showed that the distributions of burst properties are narrower in FO nuclei, such that each nucleus is characterized by bursts that are distinct in terms of the average number of spikes and latency (small values for both properties in vMGB, small number of spikes/burst with relatively long latencies in dLGN, and large number of spikes/burst and relatively short latencies in VP). HO neurons instead displayed wider ranges of burst properties, which overlapped with those in FO, but the distributions were more similar across the three HO nuclei. These results suggest that early in the sensory hierarchy the properties of bursts are determined by the sensory modality being processed. A distinguishing feature of HO nuclei is that they

receive driver input from layer V of cortex. The broader range of burst properties among HO cells, might reflect an adaptation to process or transmit the cortical information that HO cells receive from layer V, or to adjust to regional specializations in timescale dynamics observed through the neocortical hierarchy (Murray et al., 2014). Burst firing can facilitate transmission through the thalamus (Alitto et al., 2019; Hu & Agmon, 2016; Swadlow & Gusev, 2001). Bursts with more spikes, which we observed mainly in HO neurons (and in VP) have been found to activate more effectively cortical pyramidal cells and somatostatin interneurons compared to fast spiking interneurons (Hu & Agmon, 2016). Somatostatin interneurons are thought to facilitate feedforward transmission in cortex by hindering the effect of cortical feedback on distal dendrites (Tremblay et al., 2016; Wang & Yang, 2018). Thus, thalamic cells producing more spikes per burst may be more likely to engage somatostatin inhibition and enhance the transmission of thalamocortical input. Interestingly, the ratio of somatostatin to fast spiking interneurons increases from sensory to HO cortical areas (Wang & Yang, 2018), and the higher number of spikes per burst in HO thalamic cells may ensure that thalamic bursts activate the more common somatostatin interneurons in these regions.

We found that burst properties differed among the six nuclei we studied, but their distributions also overlapped, indicating that many cells in HO nuclei have properties like those in FO, and that what characterizes HO regions is a wider range of burst features. This result adds to other aspects of the functional diversity of HO thalamic regions, such as receiving excitatory and inhibitory inputs from multiple origins, expressing specific gene profiles, and having more varied responses to neuromodulators (Bickford, 2015; Bokor et al., 2005; Clascá et al., 2012; Groh et al., 2014; Phillips et al., 2019; Rovó et al., 2012; Varela, 2014). In particular, HO nuclei contain a mix of FO and HO circuits (Bickford, 2015; Guillery & Sherman, 2002; Zhou et al., 2017), and it is possible that HO neurons that have burst properties like those in FO are part of FO-like circuits within the HO nuclei.

4.2 | Comparison with previous studies of burst diversity

Consistent with our findings, LP cells were found to have a larger T current and higher density of T channels compared to dLGN (Wei et al., 2011), and VP cells had more spikes per burst compared to POm (Landisman & Connors, 2007; Slézia et al., 2011). Interestingly, POm cells fired at significantly lower frequencies (3.88 Hz) compared to VP cells (5.82 Hz) during NREM sleep slow oscillations (Slézia et al., 2011), which could be partly due to the longer latencies to burst that we observed in POm compared to VP. Although not significant in our sample, we also saw a trend for higher within-burst firing rates in VP compared to POm (Landisman & Connors, 2007; Slézia et al., 2011).

Experiments that compared bursting in different thalamic nuclei have shown that HO neurons have a higher propensity to burst (Ramcharan et al., 2005; Wei et al., 2011). By comparing additional

sensory nuclei, we have revealed new trends, showing that the distributions of spikes per burst and the latency extend to higher values in HO neurons. A study that directly compared the propensity to burst in dLGN, VP, and vMGB in macaques (Ramcharan et al., 2005), found that dLGN had the lowest proportion of spikes in bursts, consistent with our in vitro recordings in which many dLGN cells produced no rebound bursts. Long latencies like the ones we observed in dLGN can be seen in figures from previous dLGN studies (Zhan et al., 1999). In agreement with previous work, we also found a linear relation between hyperpolarization and the spike frequency of the first spikes in the burst, although we did not find a strong correlation between hyperpolarization and the number of spikes per burst. The long hyperpolarization pulses we used to ensure deinactivation of the T channels, followed by the removal of the step inhibition, may have precluded the observation of linear changes in the number of spikes per burst with hyperpolarization. However, an advantage of the experimental approach we used is that it may resemble more closely the rebound bursting induced in thalamic cells after removal of inhibition, for example, following input from TRN (Bal et al., 1995; Bal & McCormick, 1993; Crunelli et al., 2018; Fuentealba & Steriade, 2005). Evoking bursts through the injection of depolarizing current (or EPSPs) could override the latencies we observed, as depolarizing input can evoke faster bursts (Zhan et al., 1999). In fact, bursts occur at a shorter latency than tonic spikes during visual stimulation (Alitto et al., 2005; Guido et al., 1992; Lu et al., 1995; Ortuño et al., 2014). Our results suggest that conditions in which inhibitory input dominates, such as sleep, may be more likely to evoke bursts with fixed number of spikes regardless of hyperpolarization, and will be constrained by the intrinsic latencies reported here.

There is evidence of different burst propensity among TRN functional cell types defined by connectivity and molecular markers. TRN cells connected to sensory thalamic nuclei have a stronger T current and propensity to rhythmic bursting compared to HO regions of the thalamus (Clemente-Perez et al., 2017; Fernandez et al., 2018; Li et al., 2020; Martinez-Garcia et al., 2020). Although we did not find evidence of rhythmic bursting as reported in TRN cells, our work compared six nuclei under the same experimental preparation and shows that burst properties also vary among the cells of the dorsal thalamus. An interesting future study would be to investigate how burst properties in the dorsal thalamus correlate with cell connectivity with specific subtypes of TRN cells. Although most of these previous studies have been performed in rodents, a few used other species, such as tree shrews (Wei et al., 2011) and macaque monkeys (Ramcharan et al., 2005), suggesting that burst properties may constitute one more feature that adds to the molecular and connectivity profiles that seem to define the organization of the mammalian thalamus (Phillips et al., 2019).

4.3 | Mechanisms underlying burst diversity

Three genes (*Cacna1G-I*) encode the three low-voltage-activated T-type calcium channels (CaV3.1, CaV3.2, CaV3.3) that are the

primary contributors to bursting in thalamic cells (Anderson et al., 2005; Astori et al., 2011; Cain et al., 2018; Dreyfus et al., 2010; Kim et al., 2001; Talley et al., 1999). CaV3.1 is the main channel expressed in the dorsal thalamus, and recent estimates from mRNA sequencing experiments suggest increased levels of the 3.1 mRNA in LP and POm compared to dLGN and VP (Phillips et al., 2019). It is not yet known if the higher levels of mRNA translate into more CaV3.1 protein in HO thalamocortical cells, but this would be consistent with our model, which suggests that higher expression of T channels can explain why we found bursts with more spikes in HO nuclei and in VP. In addition to higher levels of *Cacna1G* expression, HO nuclei may contain more *Cacna1H* mRNA (Phillips et al., 2019) and higher levels of the CaV3.2 protein have been reported in LP compared to dLGN (Wei et al., 2011). A higher ratio of CaV3.2 to CaV3.1 channels could contribute to making HO bursts distinct due to slight differences in channel dynamics (Cain & Snutch, 2010; Kozlov et al., 1999; Xu & Clancy, 2008). Overall, the evidence points to a stronger T-channel-mediated conductance in HO nuclei and VP, and future experiments could test the contribution of specific channels, as more precise T-channel blockers become available (Choe et al., 2011). In addition to intrinsic properties, local circuit connectivity could in theory influence some burst properties, for example, the number of spikes. However, local excitatory connections between thalamocortical cells are thought to be absent in the nuclei we studied, and only the dLGN of rats contains a significant population of local interneurons (Spreafico et al., 1993), and so network effects are unlikely to explain the diversity of burst properties found in our sample.

To fully grasp the implications of our findings, we need a deeper understanding of how burst properties change during postnatal development in functionally distinct thalamic nuclei. FO and HO nuclei develop from distinct progenitor clusters in the embryo (Shi et al., 2017), which may contribute to the functional differences we observed in young rats at about 15 days of age. After birth, FO and HO sectors of the TRN appear to have similar developmental schedules in cats, but experiments are scarce (Fitzgibbon, 2007). In the dorsal thalamus, T-channel expression and conductance increase in the first postnatal days and reach mature levels around P12-13 in rodents (Perez Velazquez & Carlen, 1996; Ramoa & McCormick, 1994; Tennigkeit et al., 1998; Warren & Jones, 1997). While the age was not different between the neurons of different nuclei in our sample (P11–P18), it is possible that some HO neurons accumulate T channels more rapidly in their membranes or continue to increase their density beyond P12–13, leading to stronger LTS currents. Our finding that in LP rat age correlated with a decrease in burst latency suggests that in some nuclei bursts may be under stronger developmental control than others. The rate of insertion of T channels in the cell membrane and the changes in T-channel conductance during early development deserve further investigation and can have implications in neurodevelopmental disorders that are associated with T-channel dysfunction (Cheong & Shin, 2014; Lu et al., 2012). Critical periods of different lengths and uneven rates of maturation are important factors in the development of cortical areas (Hensch & Bilimoria, 2012; Reh et al., 2020), and the response

properties of thalamic cells may vary in coordination with (and contribute to) regional cortical development.

We did not find evidence that intrinsic properties such as membrane resistance or capacitance or other conductances, such as I_h, would explain the differences in burst properties among the nuclei we studied; however, in both FO and HO neurons, we saw a decrease in burst latency when a stronger sag voltage preceded the burst. A stronger I_h may facilitate faster oscillatory rebound bursting, emphasizing the interaction between I_h and I_t currents in dictating the oscillatory properties of thalamic cells (McCormick & Pape, 1990; Huguenard & McCormick, 2007). Conversely, our model suggested that changes in I_A could lead to bursts with less spikes and slower latencies, consistent with previous work (Amarillo et al., 2014; McCormick & Huguenard, 1992; Rush & Rinzel, 1995). However, we did not investigate potential differences in I_A across thalamic nuclei in these experiments; slow potassium channels and calcium-dependent small conductance potassium channels (SK) are weakly expressed in dorsal thalamic nuclei and their contribution to subthreshold voltages is thought to be minimal (Amarillo et al., 2014), but some of these channels have a strong influence in firing in the thalamic reticular nucleus (Cueni et al., 2008), and the study of I_A and other potassium conductances deserves further exploration.

Several neuromodulators can alter the kinetics of T-channel activation and inactivation, and the size of the T current (Huguenard, 1996; Perez-Reyes, 2003). In the hippocampus, activation of GABA_B receptors decreased, while muscarinic, serotonergic, and noradrenergic (in the cerebellum) receptors increased T currents. Shifts in the voltage dependence of the activation and inactivation curves have been studied mainly outside of the brain (cell cultures, cardiac tissue) and are controlled by second messengers and protein kinases (cAMP, protein kinase A) suggesting that T channels are under strong regulation of G-protein-coupled receptors. FO nuclei express different levels of G-protein-coupled receptors (Phillips et al., 2019) and changes in the constitutive levels of G-protein cascades (Meye et al., 2014; Seifert & Wenzel-Seifert, 2002) could determine T-channel kinetics and burst latencies. The modeling results suggest that shifts in the voltage dependence and size of T current are sufficient to induce bursts with different properties. Neuromodulators regulate several thalamic conductances (McCormick & Williamson, 1991; Pape, 1992), and an important open question is if burst properties can be dynamically regulated by neuromodulators, which would influence the strength of thalamocortical transmission and the oscillatory frequency of thalamic cells during different animal behaviors.

4.4 | Functional implications for thalamocortical transmission and oscillatory bursting

Producing bursts with more spikes may activate specific cell types in cortex and facilitate feedforward thalamocortical transmission, but there is a trade-off due to the depression properties of the thalamocortical synapse. Recovery times in the thalamocortical synapse are in the order of hundreds of miliseconds (Dittman &

Regehr, 1998; Gil et al., 1997; Tsodyks & Markram, 1997), and our model suggests that with more spikes in quick succession, the thalamocortical synapse will work at a fraction of its effectiveness. However, a depressed thalamocortical terminal does not necessarily imply weaker transmission to cortex, as transmission can be achieved through synchronicity among weak thalamocortical synapses converging onto cortical cells (Bruno & Sakmann, 2006). The latency to burst in the thalamic cells converging onto a given cortical cell could determine their synchronous firing and the subsequent activation of the cortical cell. Convergence of thalamic cells with similar latencies could facilitate synchronization and cortical activation, for example, to promote oscillatory firing in the thalamocortical network during sleep. Instead, convergence of thalamic cells with a broad range of latencies, which could occur with projections from HO nuclei or from dLGN to cortex, could lead to desynchronized inputs and reduce thalamocortical transmission. In the visual system, the level of burst desynchronization between distinct functional retinogeniculate pathways has been suggested to reduce synaptic competition and contribute to the segregation of ON–OFF pathways during development (Gjorgjieva et al., 2009; Torborg et al., 2005). It is possible that the wide range of latencies we found in dLGN and HO thalamic nuclei will have developmental implications, by promoting desynchronization and the segregation of activity in different functional pathways. Thus, intrinsic properties (such as the latency to burst) may combine with circuit features (such as connections with TRN and the convergence of thalamic relay cells on cortical cells), to facilitate or preclude synchronous firing at specific frequencies in functional groups of thalamocortical cells. Likewise, the longer latencies we observed in HO nuclei could provide additional recovery time during rebound bursting and partially compensate the synaptic depletion of neurotransmitter. Although the latencies are short in many FO cells, the lower number of spikes per burst in dLGN and vMGB would prevent synaptic depletion and preserve the effectiveness of upcoming bursts.

The burst latency values we report identify an intrinsic mechanism that may contribute to limit the burst oscillatory frequency of thalamocortical cells during rebound bursting, particularly in dLGN and HO cells. It is possible that bursts driven by direct depolarization are less influenced by latency and could reach higher oscillatory frequencies; T-channel dynamics are also expected to be faster in vivo, where time constants can be several times those recorded at room temperature in vitro (Huguenard, 1996). Nonetheless, several studies described frequency limits that could be explained by our findings. dLGN cells can follow frequencies of up to about 20 Hz during visual stimulation while in burst mode (Guido et al., 1992) and an upper limit of about 20 Hz has been reported for CaV3.1 and CaV3.2 currents in cell cultures (Kozlov et al., 1999). Even during sleep, when the burst rate is highest, cells in the dorsal thalamus have been found to fire bursts sparsely and nonrhythmically or with frequencies below 10 Hz (Deschênes et al., 1984; Dossi et al., 1992; Ramcharan et al., 2000, 2005; Slézia et al., 2011; Varela & Wilson, 2020). Cells with the longest latencies (in HO and dLGN), may fail to follow the cycle-to-cycle dynamics of spindle oscillations (10–15 Hz), but these cells may be particularly suited to contribute to slow and delta oscillations in NREM sleep (David et al., 2013; Slézia et al., 2011; Steriade et al., 1993). Future thalamocortical network models that investigate rebound spiking could reveal the implications of the results reported here for thalamocortical transmission under different oscillatory regimes and in the context of behavioral states defined by neuromodulators (Hasselmo et al., 2020; Jaramillo et al., 2019).

CONFLICT OF INTEREST

The authors declare that they have no conflict of interest.

AUTHOR CONTRIBUTIONS

All authors had full access to the data and take responsibility for the integrity of the data and accuracy of data analysis. Nidhi Vasant Desai and Carmen Varela wrote the paper; Nidhi Vasant Desai wrote the code, analyzed the data and prepared the figures; Carmen Varela recorded the in vitro data.

PEER REVIEW

The peer review history for this article is available at https://publons.com/publon/10.1002/cne.25141.

DATA AVAILABILITY STATEMENT

The data used in this study is available from the corresponding author upon request.

ORCID

Carmen Varela https://orcid.org/0000-0003-0398-2567

REFERENCES

Alitto, H., Rathbun, D. L., Vandeleest, J. J., Alexander, P. C., & Usrey, W. M. (2019). The augmentation of Retinogeniculate communication during thalamic burst mode. *The Journal of Neuroscience: The Official Journal of the Society for Neuroscience, 39*(29), 5697–5710. https://doi.org/10.1523/JNEUROSCI.2320-18.2019

Alitto, H. J., Weyand, T. G., & Usrey, W. M. (2005). Distinct properties of stimulus-evoked bursts in the lateral geniculate nucleus. *The Journal of Neuroscience: The Official Journal of the Society for Neuroscience, 25*(2), 514–523. https://doi.org/10.1523/JNEUROSCI.3369-04.2005

Amarillo, Y., Zagha, E., Mato, G., Rudy, B., & Nadal, M. S. (2014). The interplay of seven subthreshold conductances controls the resting membrane potential and the oscillatory behavior of thalamocortical neurons. *Journal of Neurophysiology, 112*(2), 393–410. https://doi.org/10.1152/jn.00647.2013

Anderson, M. P., Mochizuki, T., Xie, J., Fischler, W., Manger, J. P., Talley, E. M., Scammell, T. E., & Tonegawa, S. (2005). Thalamic Cav3.1 T-type Ca2+ channel plays a crucial role in stabilizing sleep. *Proceedings of the National Academy of Sciences of the United States of America, 102*(5), 1743–1748. https://doi.org/10.1073/pnas.0409644102

Astori, S., Wimmer, R. D., Prosser, H. M., Corti, C., Corsi, M., Liaudet, N., Volterra, A., Franken, P., Adelman, J. P., & Lüthi, A. (2011). The Ca(V)3.3 calcium channel is the major sleep spindle pacemaker in thalamus. *Proceedings of the National Academy of Sciences of the United States of America*, 108(33), 13823–13828. https://doi.org/10.1073/pnas.1105115108

Bal, T., & McCormick, D. A. (1993). Mechanisms of oscillatory activity in Guinea-pig nucleus reticularis thalami in vitro: A mammalian pacemaker. *The Journal of Physiology*, 468, 669–691. https://doi.org/10.1113/jphysiol.1993.sp019794

Bal, T., von Krosigk, M., & McCormick, D. A. (1995). Role of the ferret perigeniculate nucleus in the generation of synchronized oscillations in vitro. *The Journal of Physiology*, 483(Pt 3), 665–685. https://doi.org/10.1113/jphysiol.1995.sp020613

Barthó, P., Freund, T. F., & Acsády, L. (2002). Selective GABAergic innervation of thalamic nuclei from zona incerta. *The European Journal of Neuroscience*, 16(6), 999–1014. https://doi.org/10.1046/j.1460-9568.2002.02157.x

Benita, J. M., Guillamon, A., Deco, G., & Sanchez-Vives, M. V. (2012). Synaptic depression and slow oscillatory activity in a biophysical network model of the cerebral cortex. *Frontiers in Computational Neuroscience*, 6, 64. https://doi.org/10.3389/fncom.2012.00064

Bickford, M. E. (2015). Thalamic circuit diversity: Modulation of the driver/modulator framework. *Frontiers in Neural Circuits*, 9, 86. https://doi.org/10.3389/fncir.2015.00086

Bokor, H., Frère, S. G. A., Eyre, M. D., Slézia, A., Ulbert, I., Lüthi, A., & Acsády, L. (2005). Selective GABAergic control of higher-order thalamic relays. *Neuron*, 45(6), 929–940. https://doi.org/10.1016/j.neuron.2005.01.048

Bruno, R. M., & Sakmann, B. (2006). Cortex is driven by weak but synchronously active thalamocortical synapses. *Science (New York, N.Y.)*, 312(5780), 1622–1627. https://doi.org/10.1126/science.1124593

Cain, S. M., & Snutch, T. P. (2010). Contributions of T-type calcium channel isoforms to neuronal firing. *Channels (Austin, Tex.)*, 4(6), 475–482. https://doi.org/10.4161/chan.4.6.14106

Cain, S. M., Tyson, J. R., Choi, H.-B., Ko, R., Lin, P. J. C., LeDue, J. M., Powell, K. L., Bernier, L.-P., Rungta, R. L., Yang, Y., Cullis, P. R., O'Brien, T. J., MacVicar, B. A., & Snutch, T. P. (2018). CaV 3.2 drives sustained burst-firing, which is critical for absence seizure propagation in reticular thalamic neurons. *Epilepsia*, 59(4), 778–791. https://doi.org/10.1111/epi.14018

Cazade, M., Bidaud, I., Lory, P., & Chemin, J. (2017). Activity-dependent regulation of T-type calcium channels by submembrane calcium ions. *eLife*, 6, e22331. https://doi.org/10.7554/eLife.22331

Cheong, E., & Shin, H.-S. (2014). T-type Ca2+ channels in absence epilepsy. *Pflugers Archiv: European Journal of Physiology*, 466(4), 719–734. https://doi.org/10.1007/s00424-014-1461-y

Choe, W., Messinger, R. B., Leach, E., Eckle, V.-S., Obradovic, A., Salajegheh, R., Jevtovic-Todorovic, V., & Todorovic, S. M. (2011). TTA-P2 is a potent and selective blocker of T-type calcium channels in rat sensory neurons and a novel antinociceptive agent. *Molecular Pharmacology*, 80(5), 900–910. https://doi.org/10.1124/mol.111.073205

Chung, J. M., Huguenard, J. R., & Prince, D. A. (1993). Transient enhancement of low-threshold calcium current in thalamic relay neurons after corticectomy. *Journal of Neurophysiology*, 70(1), 20–27. https://doi.org/10.1152/jn.1993.70.1.20

Clascá, F., Rubio-Garrido, P., & Jabaudon, D. (2012). Unveiling the diversity of thalamocortical neuron subtypes. *The European Journal of Neuroscience*, 35(10), 1524–1532. https://doi.org/10.1111/j.1460-9568.2012.08033.x

Clemente-Perez, A., Makinson, S. R., Higashikubo, B., Brovarney, S., Cho, F. S., Urry, A., Holden, S. S., Wimer, M., Dávid, C., Fenno, L. E., Acsády, L., Deisseroth, K., & Paz, J. T. (2017). Distinct thalamic reticular cell types differentially modulate Normal and pathological cortical rhythms. *Cell Reports*, 19(10), 2130–2142. https://doi.org/10.1016/j.celrep.2017.05.044

Crunelli, V., Lőrincz, M. L., Connelly, W. M., David, F., Hughes, S. W., Lambert, R. C., Leresche, N., & Errington, A. C. (2018). Dual function of thalamic low-vigilance state oscillations: Rhythm-regulation and plasticity. *Nature Reviews Neuroscience*, 19(2), 107–118. https://doi.org/10.1038/nrn.2017.151

Cueni, L., Canepari, M., Luján, R., Emmenegger, Y., Watanabe, M., Bond, C. T., Franken, P., Adelman, J. P., & Lüthi, A. (2008). T-type Ca2+ channels, SK2 channels and SERCAs gate sleep-related oscillations in thalamic dendrites. *Nature Neuroscience*, 11(6), 683–692. https://doi.org/10.1038/nn.2124

David, F., Schmiedt, J. T., Taylor, H. L., Orban, G., Di Giovanni, G., Uebele, V. N., Renger, J. J., Lambert, R. C., Leresche, N., & Crunelli, V. (2013). Essential thalamic contribution to slow waves of natural sleep. *The Journal of Neuroscience: The Official Journal of the Society for Neuroscience*, 33(50), 19599–19610. https://doi.org/10.1523/JNEUROSCI.3169-13.2013

Deschênes, M., Paradis, M., Roy, J. P., & Steriade, M. (1984). Electrophysiology of neurons of lateral thalamic nuclei in cat: Resting properties and burst discharges. *Journal of Neurophysiology*, 51(6), 1196–1219. https://doi.org/10.1152/jn.1984.51.6.1196

Destexhe, A., Bal, T., McCormick, D. A., & Sejnowski, T. J. (1996). Ionic mechanisms underlying synchronized oscillations and propagating waves in a model of ferret thalamic slices. *Journal of Neurophysiology*, 76(3), 2049–2070. https://doi.org/10.1152/jn.1996.76.3.2049

Dittman, J. S., & Regehr, W. G. (1998). Calcium dependence and recovery kinetics of presynaptic depression at the climbing fiber to Purkinje cell synapse. *The Journal of Neuroscience*, 18(16), 6147–6162. https://doi.org/10.1523/JNEUROSCI.18-16-06147.1998

Dossi, R. C., Nuñez, A., & Steriade, M. (1992). Electrophysiology of a slow (0.5-4 Hz) intrinsic oscillation of cat thalamocortical neurones in vivo. *The Journal of Physiology*, 447, 215–234. https://doi.org/10.1113/jphysiol.1992.sp018999

Dreyfus, F. M., Tscherter, A., Errington, A. C., Renger, J. J., Shin, H.-S., Uebele, V. N., Crunelli, V., Lambert, R. C., & Leresche, N. (2010). Selective T-type Calcium Channel block in thalamic neurons reveals channel redundancy and physiological impact of ITwindow. *The Journal of Neuroscience*, 30(1), 99–109. https://doi.org/10.1523/JNEUROSCI.4305-09.2010

Fernandez, L. M., Vantomme, G., Osorio-Forero, A., Cardis, R., Béard, E., & Lüthi, A. (2018). Thalamic reticular control of local sleep in mouse sensory cortex. *eLife*, 7, e39111. https://doi.org/10.7554/eLife.39111

Fitzgibbon, T. (2007). Do first order and higher order regions of the thalamic reticular nucleus have different developmental timetables? *Experimental Neurology*, 204(1), 339–354. https://doi.org/10.1016/j.expneurol.2006.11.012

Fourment, A., Hirsch, J. C., Marc, M. E., & Guidet, C. (1984). Modulation of postsynaptic activities of thalamic lateral geniculate neurons by spontaneous changes in number of retinal inputs in chronic cats. 1. Input-output relations. *Neuroscience*, 12(2), 453–464. https://doi.org/10.1016/0306-4522(84)90065-4

Fuentealba, P., & Steriade, M. (2005). The reticular nucleus revisited: Intrinsic and network properties of a thalamic pacemaker. *Progress in Neurobiology*, 75(2), 125–141. https://doi.org/10.1016/j.pneurobio.2005.01.002

Gil, Z., Connors, B. W., & Amitai, Y. (1997). Differential regulation of neocortical synapses by neuromodulators and activity. *Neuron*, 19(3), 679–686. https://doi.org/10.1016/S0896-6273(00)80380-3

Gjorgjieva, J., Toyoizumi, T., & Eglen, S. J. (2009). Burst-time-dependent plasticity robustly guides ON/OFF segregation in the lateral geniculate nucleus. *PLoS Computational Biology*, 5(12), e1000618. https://doi.org/10.1371/journal.pcbi.1000618

Groh, A., Bokor, H., Mease, R. A., Plattner, V. M., Hangya, B., Stroh, A., Deschenes, M., & Acsády, L. (2014). Convergence of cortical and sensory

driver inputs on single thalamocortical cells. *Cerebral Cortex (New York, N.Y.: 1991)*, *24*(12), 3167–3179. https://doi.org/10.1093/cercor/bht173

Guido, W., Lu, S. M., & Sherman, S. M. (1992). Relative contributions of burst and tonic responses to the receptive field properties of lateral geniculate neurons in the cat. *Journal of Neurophysiology*, *68*(6), 2199–2211. https://doi.org/10.1152/jn.1992.68.6.2199

Guido, W., & Weyand, T. (1995). Burst responses in thalamic relay cells of the awake behaving cat. *Journal of Neurophysiology*, *74*(4), 1782–1786.

Guillery, R. W., & Sherman, S. M. (2002). Thalamic relay functions and their role in corticocortical communication: Generalizations from the visual system. *Neuron*, *33*(2), 163–175. https://doi.org/10.1016/s0896-6273(01)00582-7

Gutierrez, C., Cox, C. L., Rinzel, J., & Sherman, S. M. (2001). Dynamics of low-threshold spike activation in relay neurons of the cat lateral geniculate nucleus. *The Journal of Neuroscience: The Official Journal of the Society for Neuroscience*, *21*(3), 1022–1032.

Halassa, M. M., & Acsády, L. (2016). Thalamic inhibition: Diverse sources, diverse scales. *Trends in Neurosciences*, *39*(10), 680–693. https://doi.org/10.1016/j.tins.2016.08.001

Halassa, M. M., & Sherman, S. M. (2019). Thalamocortical circuit motifs: A general framework. *Neuron*, *103*(5), 762–770. https://doi.org/10.1016/j.neuron.2019.06.005

Hasselmo, M. E., Alexander, A. S., Hoyland, A., Robinson, J. C., Bezaire, M. J., Chapman, G. W., Saudargiene, A., Carstensen, L. C., & Dannenberg, H. (2020). The unexplored territory of neural models: Potential guides for exploring the function of metabotropic Neuromodulation. *Neuroscience*. *456*, 143–158. https://doi.org/10.1016/j.neuroscience.2020.03.048

Hensch, T. K., & Bilimoria, P. M. (2012). Re-opening windows: Manipulating critical periods for brain development. *Cerebrum: The Dana Forum on Brain Science*, 2012.

Hodgkin, A. L., & Huxley, A. F. (1952). A quantitative description of membrane current and its application to conduction and excitation in nerve. *The Journal of Physiology*, *117*(4), 500–544. https://doi.org/10.1113/jphysiol.1952.sp004764

Hu, H., & Agmon, A. (2016). Differential excitation of distally versus proximally targeting cortical interneurons by unitary thalamocortical bursts. *The Journal of Neuroscience: The Official Journal of the Society for Neuroscience*, *36*(26), 6906–6916. https://doi.org/10.1523/JNEUROSCI.0739-16.2016

Huguenard, J. R. (1996). Low-threshold calcium currents in central nervous system neurons. *Annual Review of Physiology*, *58*, 329–348. https://doi.org/10.1146/annurev.ph.58.030196.001553

Huguenard, J. R., & McCormick, D. A. (2007). Thalamic synchrony and dynamic regulation of global forebrain oscillations. *Trends in Neurosciences*, *30*(7), 350–356. https://doi.org/10.1016/j.tins.2007.05.007

Jahnsen, H., & Llinás, R. (1984a). Voltage-dependent burst-to-tonic switching of thalamic cell activity: An in vitro study. *Archives Italiennes de Biologie*, *122*(1), 73–82.

Jahnsen, H., & Llinás, R. (1984b). Electrophysiological properties of Guinea-pig thalamic neurones: An in vitro study. *The Journal of Physiology*, *349*, 205–226. https://doi.org/10.1113/jphysiol.1984.sp015153

Jaramillo, J., Mejias, J. F., & Wang, X.-J. (2019). Engagement of Pulvino-cortical feedforward and feedback pathways in cognitive computations. *Neuron*, *101*(2), 321–336.e9. https://doi.org/10.1016/j.neuron.2018.11.023

Jones, E. G. (1998). Viewpoint: The core and matrix of thalamic organization. *Neuroscience*, *85*(2), 331–345. https://doi.org/10.1016/S0306-4522(97)00581-2

Kim, D., Song, I., Keum, S., Lee, T., Jeong, M. J., Kim, S. S., McEnery, M. W., & Shin, H. S. (2001). Lack of the burst firing of thalamocortical relay neurons and resistance to absence seizures in mice lacking alpha(1G) T-type Ca(2+) channels. *Neuron*, *31*(1), 35–45. https://doi.org/10.1016/s0896-6273(01)00343-9

Kozlov, A. S., McKenna, F., Lee, J.-H., Cribbs, L. L., Perez-Reyes, E., Feltz, A., & Lambert, R. C. (1999). Distinct kinetics of cloned T-type Ca2 + channels lead to differential Ca2 + entry and frequency-dependence during mock action potentials. *European Journal of Neuroscience*, *11*(12), 4149–4158. https://doi.org/10.1046/j.1460-9568.1999.00841.x

Krahe, R., & Gabbiani, F. (2004). Burst firing in sensory systems. *Nature Reviews. Neuroscience*, *5*(1), 13–23. https://doi.org/10.1038/nrn1296

Kramer, M. A. & Eden U. T. (2016). Case Studies in Neural Data Analysis: A Guide for the Practicing Neuroscientist. The MIT Press.

Landisman, C. E., & Connors, B. W. (2007). VPM and PoM nuclei of the rat somatosensory thalamus: Intrinsic neuronal properties and corticothalamic feedback. *Cerebral Cortex (New York, N.Y.: 1991)*, *17*(12), 2853–2865. https://doi.org/10.1093/cercor/bhm025

Li, J., Bickford, M. E., & Guido, W. (2003). Distinct firing properties of higher order thalamic relay neurons. *Journal of Neurophysiology*, *90*(1), 291–299. https://doi.org/10.1152/jn.01163.2002

Li, Y., Lopez-Huerta, V. G., Adiconis, X., Levandowski, K., Choi, S., Simmons, S. K., Arias-Garcia, M. A., Guo, B., Yao, A. Y., Blosser, T. R., Wimmer, R. D., Aida, T., Atamian, A., Naik, T., Sun, X., Bi, D., Malhotra, D., Hession, C. C., Shema, R., … Feng, G. (2020). Distinct subnetworks of the thalamic reticular nucleus. *Nature*, *583*(7818), 819–824. https://doi.org/10.1038/s41586-020-2504-5

Llinás, R. R. (2014). Intrinsic electrical properties of mammalian neurons and CNS function: A historical perspective. *Frontiers in Cellular Neuroscience*, *8*. https://doi.org/10.3389/fncel.2014.00320

Llinás, R. R., & Steriade, M. (2006). Bursting of thalamic neurons and states of vigilance. *Journal of Neurophysiology*, *95*(6), 3297–3308. https://doi.org/10.1152/jn.00166.2006

Lu, A. T.-H., Dai, X., Martinez-Agosto, J. A., & Cantor, R. M. (2012). Support for calcium channel gene defects in autism spectrum disorders. *Molecular Autism*, *3*(1), 18. https://doi.org/10.1186/2040-2392-3-18

Lu, S. M., Guido, W., Vaughan, J. W., & Sherman, S. M. (1995). Latency variability of responses to visual stimuli in cells of the cat's lateral geniculate nucleus. *Experimental Brain Research*, *105*(1), 7–17.

Lüthi, A., & McCormick, D. A. (1998). H-current: Properties of a neuronal and network pacemaker. *Neuron*, *21*(1), 9–12. https://doi.org/10.1016/S0896-6273(00)80509-7

Martinez-Garcia, R. I., Voelcker, B., Zaltsman, J. B., Patrick, S. L., Stevens, T. R., Connors, B. W., & Cruikshank, S. J. (2020). Two dynamically distinct circuits drive inhibition in the sensory thalamus. *Nature*, *583*(7818), 813–818. https://doi.org/10.1038/s41586-020-2512-5

McCormick, D. A., & Huguenard, J. R. (1992). A model of the electrophysiological properties of thalamocortical relay neurons. *Journal of Neurophysiology*, *68*(4), 1384–1400. https://doi.org/10.1152/jn.1992.68.4.1384

McCormick, D. A., & Pape, H. C. (1990). Properties of a hyperpolarization-activated cation current and its role in rhythmic oscillation in thalamic relay neurones. *The Journal of Physiology*, *431*, 291–318. https://doi.org/10.1113/jphysiol.1990.sp018331

McCormick, D. A., & Williamson, A. (1991). Modulation of neuronal firing mode in cat and Guinea pig LGNd by histamine: Possible cellular mechanisms of histaminergic control of arousal. *The Journal of Neuroscience: The Official Journal of the Society for Neuroscience*, *11*(10), 3188–3199.

Meye, F. J., Ramakers, G. M. J., & Adan, R. A. H. (2014). The vital role of constitutive GPCR activity in the mesolimbic dopamine system. *Translational Psychiatry*, *4*(2), e361–e361. https://doi.org/10.1038/tp.2013.130

Murray, J. D., Bernacchia, A., Freedman, D. J., Romo, R., Wallis, J. D., Cai, X., Padoa-Schioppa, C., Pasternak, T., Seo, H., Lee, D., & Wang, X.-J. (2014). A hierarchy of intrinsic timescales across primate cortex. *Nature Neuroscience*, *17*(12), 1661–1663. https://doi.org/10.1038/nn.3862

Nicolelis, M. A. L. (2005). Computing with thalamocortical ensembles during different behavioural states. *The Journal of Physiology*, *566*(Pt 1), 37–47. https://doi.org/10.1113/jphysiol.2005.083709

Ortuño, T., Grieve, K. L., Cao, R., Cudeiro, J., & Rivadulla, C. (2014). Bursting thalamic responses in awake monkey contribute to visual detection and are modulated by corticofugal feedback. *Frontiers in Behavioral Neuroscience*, *8*, 198. https://doi.org/10.3389/fnbeh.2014.00198

Pape, H. C. (1992). Adenosine promotes burst activity in Guinea-pig geniculocortical neurones through two different ionic mechanisms. *The Journal of Physiology*, *447*, 729–753. https://doi.org/10.1113/jphysiol.1992.sp019026

Perez Velazquez, J. L., & Carlen, P. L. (1996). Development of firing patterns and electrical properties in neurons of the rat ventrobasal thalamus. *Developmental Brain Research*, *91*(2), 164–170. https://doi.org/10.1016/0165-3806(95)00171-9

Perez-Reyes, E. (2003). Molecular physiology of low-voltage-activated t-type calcium channels. *Physiological Reviews*, *83*(1), 117–161. https://doi.org/10.1152/physrev.00018.2002

Phillips, J. W., Schulmann, A., Hara, E., Winnubst, J., Liu, C., Valakh, V., Wang, L., Shields, B. C., Korff, W., Chandrashekar, J., Lemire, A. L., Mensh, B., Dudman, J. T., Nelson, S. B., & Hantman, A. W. (2019). A repeated molecular architecture across thalamic pathways. *Nature Neuroscience*, *22*(11), 1925–1935. https://doi.org/10.1038/s41593-019-0483-3

Prasad, J. A., Carroll, B. J., & Sherman, S. M. (2020). Layer 5 Corticofugal projections from diverse cortical areas: Variations on a pattern of thalamic and Extrathalamic targets. *The Journal of Neuroscience: The Official Journal of the Society for Neuroscience*, *40*(30), 5785–5796. https://doi.org/10.1523/JNEUROSCI.0529-20.2020

Ramcharan, E. J., Gnadt, J. W., & Sherman, S. M. (2000). Burst and tonic firing in thalamic cells of unanesthetized, behaving monkeys. *Visual Neuroscience*, *17*(1), 55–62. https://doi.org/10.1017/s0952523800171056

Ramcharan, E. J., Gnadt, J. W., & Sherman, S. M. (2005). Higher-order thalamic relays burst more than first-order relays. *Proceedings of the National Academy of Sciences of the United States of America*, *102*(34), 12236–12241. https://doi.org/10.1073/pnas.0502843102

Ramoa, A. S., & McCormick, D. A. (1994). Developmental changes in electrophysiological properties of LGNd neurons during reorganization of retinogeniculate connections. *The Journal of Neuroscience: The Official Journal of the Society for Neuroscience*, *14*(4), 2089–2097.

Reh, R. K., Dias, B. G., Nelson, C. A., Kaufer, D., Werker, J. F., Kolb, B., Levine, J. D., & Hensch, T. K. (2020). Critical period regulation across multiple timescales. *Proceedings of the National Academy of Sciences*, *117*(38), 23242–23251. https://doi.org/10.1073/pnas.1820836117

Reinagel, P., Godwin, D., Sherman, S. M., & Koch, C. (1999). Encoding of visual information by LGN bursts. *Journal of Neurophysiology*, *81*(5), 2558–2569. https://doi.org/10.1152/jn.1999.81.5.2558

Rovó, Z., Ulbert, I., & Acsády, L. (2012). Drivers of the primate thalamus. *The Journal of Neuroscience: The Official Journal of the Society for Neuroscience*, *32*(49), 17894–17908. https://doi.org/10.1523/JNEUROSCI.2815-12.2012

Rush, M. E., & Rinzel, J. (1995). The potassium A-current, low firing rates and rebound excitation in Hodgkin-Huxley models. *Bulletin of Mathematical Biology*, *57*(6), 899–929. https://doi.org/10.1007/BF02458299

Seifert, R., & Wenzel-Seifert, K. (2002). Constitutive activity of G-protein-coupled receptors: Cause of disease and common property of wild-type receptors. *Naunyn-Schmiedeberg's Archives of Pharmacology*, *366*(5), 381–416. https://doi.org/10.1007/s00210-002-0588-0

Sherfey, J. S., Soplata, A. E., Ardid, S., Roberts, E. A., Stanley, D. A., Pittman-Polletta, B. R., & Kopell, N. J. (2018). DynaSim: A MATLAB toolbox for neural modeling and simulation. *Frontiers in Neuroinformatics*, *12*, 10. https://doi.org/10.3389/fninf.2018.00010

Sherman, S. M., & Guillery, R. W. (2001). *Exploring the thalamus*. Elsevier.

Sherman, S. M., & Guillery, R. W. (2011). Distinct functions for direct and transthalamic corticocortical connections. *Journal of Neurophysiology*, *106*(3), 1068–1077. https://doi.org/10.1152/jn.00429.2011

Sherman, S. M. (2001). A wake-up call from the thalamus. *Nature Neuroscience*, *4*(4), 344–346. https://doi.org/10.1038/85973

Shi, W., Xianyu, A., Han, Z., Tang, X., Li, Z., Zhong, H., Mao, T., Huang, K., & Shi, S.-H. (2017). Ontogenetic establishment of order-specific nuclear organization in the mammalian thalamus. *Nature Neuroscience*, *20*(4), 516–528. https://doi.org/10.1038/nn.4519

Sirota, A., Csicsvari, J., Buhl, D., & Buzsáki, G. (2003). Communication between neocortex and hippocampus during sleep in rodents. *Proceedings of the National Academy of Sciences of the United States of America*, *100*(4), 2065–2069. https://doi.org/10.1073/pnas.0437938100

Slézia, A., Hangya, B., Ulbert, I., & Acsády, L. (2011). Phase advancement and nucleus-specific timing of thalamocortical activity during slow cortical oscillation. *The Journal of Neuroscience: The Official Journal of the Society for Neuroscience*, *31*(2), 607–617. https://doi.org/10.1523/JNEUROSCI.3375-10.2011

Soplata, A. E., McCarthy, M. M., Sherfey, J., Lee, S., Purdon, P. L., Brown, E. N., & Kopell, N. (2017). Thalamocortical control of propofol phase-amplitude coupling. *PLoS Computational Biology*, *13*(12), e1005879. https://doi.org/10.1371/journal.pcbi.1005879

Spreafico, R., de Biasi, S., Amadeo, A., & de Blas, A. L. (1993). GABAA-receptor immunoreactivity in the rat dorsal thalamus: An ultrastructural investigation. *Neuroscience Letters*, *158*(2), 232–236. https://doi.org/10.1016/0304-3940(93)90272-m

Staresina, B. P., Bergmann, T. O., Bonnefond, M., van der Meij, R., Jensen, O., Deuker, L., Elger, C. E., Axmacher, N., & Fell, J. (2015). Hierarchical nesting of slow oscillations, spindles and ripples in the human hippocampus during sleep. *Nature Neuroscience*, *18*(11), 1679–1686. https://doi.org/10.1038/nn.4119

Steriade, M., Deschênes, M., Domich, L., & Mulle, C. (1985). Abolition of spindle oscillations in thalamic neurons disconnected from nucleus reticularis thalami. *Journal of Neurophysiology*, *54*(6), 1473–1497. https://doi.org/10.1152/jn.1985.54.6.1473

Steriade, M., Domich, L., Oakson, G., & Deschênes, M. (1987). The deafferented reticular thalamic nucleus generates spindle rhythmicity. *Journal of Neurophysiology*, *57*(1), 260–273. https://doi.org/10.1152/jn.1987.57.1.260

Steriade, M., McCormick, D. A., & Sejnowski, T. J. (1993). Thalamocortical oscillations in the sleeping and aroused brain. *Science (New York, N.Y.)*, *262*(5134), 679–685.

Suzuki, S., & Rogawski, M. A. (1989). T-type calcium channels mediate the transition between tonic and phasic firing in thalamic neurons. *Proceedings of the National Academy of Sciences of the United States of America*, *86*(18), 7228–7232. https://doi.org/10.1073/pnas.86.18.7228

Swadlow, H. A., & Gusev, A. G. (2001). The impact of "bursting" thalamic impulses at a neocortical synapse. *Nature Neuroscience*, *4*(4), 402–408. https://doi.org/10.1038/86054

Talley, E. M., Cribbs, L. L., Lee, J. H., Daud, A., Perez-Reyes, E., & Bayliss, D. A. (1999). Differential distribution of three members of a gene family encoding low voltage-activated (T-type) calcium channels. *The Journal of Neuroscience: The Official Journal of the Society for Neuroscience*, *19*(6), 1895–1911.

Tennigkeit, F., Schwarz, D. W. F., & Puil, E. (1998). Postnatal development of signal generation in auditory thalamic neurons. *Developmental Brain Research*, *109*(2), 255–263.

Torborg, C. L., Hansen, K. A., & Feller, M. B. (2005). High frequency, synchronized bursting drives eye-specific segregation of retinogeniculate projections. *Nature Neuroscience*, *8*(1), 72–78. https://doi.org/10.1038/nn1376

Tremblay, R., Lee, S., & Rudy, B. (2016). GABAergic interneurons in the neocortex: From cellular properties to circuits. *Neuron*, *91*(2), 260–292. https://doi.org/10.1016/j.neuron.2016.06.033

Tsakiridou, E., Bertollini, L., de Curtis, M., Avanzini, G., & Pape, H. C. (1995). Selective increase in T-type calcium conductance of reticular thalamic neurons in a rat model of absence epilepsy. *The Journal of Neuroscience: The Official Journal of the Society for Neuroscience*, 15(4), 3110–3117.

Tsodyks, M. V., & Markram, H. (1997). The neural code between neocortical pyramidal neurons depends on neurotransmitter release probability. *Proceedings of the National Academy of Sciences*, 94(2), 719–723. https://doi.org/10.1073/pnas.94.2.719

Varela, C., & Sherman, S. M. (2007). Differences in response to muscarinic activation between first and higher order thalamic relays. *Journal of Neurophysiology*, 98(6), 3538–3547. https://doi.org/10.1152/jn.00578.2007

Varela, C., & Sherman, S. M. (2009). Differences in response to serotonergic activation between first and higher order thalamic nuclei. *Cerebral Cortex (New York, N.Y.: 1991)*, 19(8), 1776–1786. https://doi.org/10.1093/cercor/bhn208

Varela, C. (2014). Thalamic neuromodulation and its implications for executive networks. *Frontiers in Neural Circuits*, 8, 69. https://doi.org/10.3389/fncir.2014.00069

Varela, C., & Wilson, M. A. (2020). MPFC spindle cycles organize sparse thalamic activation and recently active CA1 cells during non-REM sleep. *eLife*, 9, e48881. https://doi.org/10.7554/eLife.48881

Viaene, A. N., Petrof, I., & Sherman, S. M. (2011a). Synaptic properties of thalamic input to layers 2/3 and 4 of primary somatosensory and auditory cortices. *Journal of Neurophysiology*, 105(1), 279–292. https://doi.org/10.1152/jn.00747.2010

Viaene, A. N., Petrof, I., & Sherman, S. M. (2011b). Synaptic properties of thalamic input to the subgranular layers of primary somatosensory and auditory cortices in the mouse. *The Journal of Neuroscience: The Official Journal of the Society for Neuroscience*, 31(36), 12738–12747. https://doi.org/10.1523/JNEUROSCI.1565-11.2011

Viaene, A. N., Petrof, I., & Sherman, S. M. (2011c). Properties of the thalamic projection from the posterior medial nucleus to primary and secondary somatosensory cortices in the mouse. *Proceedings of the National Academy of Sciences of the United States of America*, 108(44), 18156–18161. https://doi.org/10.1073/pnas.1114828108

Wang, X., Wei, Y., Vaingankar, V., Wang, Q., Koepsell, K., Sommer, F. T., & Hirsch, J. A. (2007). Feedforward excitation and inhibition evoke dual modes of firing in the cat's visual thalamus during naturalistic viewing. *Neuron*, 55(3), 465–478. https://doi.org/10.1016/j.neuron.2007.06.039

Wang, X.-J., & Yang, G. R. (2018). A disinhibitory circuit motif and flexible information routing in the brain. *Current Opinion in Neurobiology*, 49, 75–83. https://doi.org/10.1016/j.conb.2018.01.002

Warren, R. A., & Jones, E. G. (1997). Maturation of neuronal form and function in a mouse Thalamo-cortical circuit. *Journal of Neuroscience*, 17(1), 277–295. https://doi.org/10.1523/JNEUROSCI.17-01-00277.1997

Wei, H., Bonjean, M., Petry, H. M., Sejnowski, T. J., & Bickford, M. E. (2011). Thalamic burst firing propensity: A comparison of the dorsal lateral geniculate and pulvinar nuclei in the tree shrew. *The Journal of Neuroscience: The Official Journal of the Society for Neuroscience*, 31(47), 17287–17299. https://doi.org/10.1523/JNEUROSCI.6431-10.2011

Weyand, T. G., Boudreaux, M., & Guido, W. (2001). Burst and tonic response modes in thalamic neurons during sleep and wakefulness. *Journal of Neurophysiology*, 85(3), 1107–1118.

Whitmire, C. J., Waiblinger, C., Schwarz, C., & Stanley, G. B. (2016). Information coding through adaptive gating of synchronized thalamic bursting. *Cell Reports*, 14(4), 795–807. https://doi.org/10.1016/j.celrep.2015.12.068

Xu, J., & Clancy, C. E. (2008). Ionic mechanisms of endogenous bursting in CA3 hippocampal pyramidal neurons: A model study. *PLoS One*, 3(4), e2056. https://doi.org/10.1371/journal.pone.0002056

Zhan, X. J., Cox, C. L., Rinzel, J., & Sherman, S. M. (1999). Current clamp and modeling studies of low-threshold calcium spikes in cells of the cat's lateral geniculate nucleus. *Journal of Neurophysiology*, 81(5), 2360–2373. https://doi.org/10.1152/jn.1999.81.5.2360

Zhou, N. A., Maire, P. S., Masterson, S. P., & Bickford, M. E. (2017). The mouse pulvinar nucleus: Organization of the tectorecipient zones. *Visual Neuroscience*, 34, E011. https://doi.org/10.1017/S0952523817000050